

Correlation effects in the Magnetic properties and nonequilibrium quantum dynamics of spinor Bose Einstein Condensates

A Thesis

submitted to

Indian Institute of Science Education and Research Pune
in partial fulfillment of the requirements for the
BS-MS Dual Degree Programme

by

Kush Mohan Mittal



Indian Institute of Science Education and Research Pune
Dr. Homi Bhabha Road,
Pashan, Pune 411008, INDIA.

May, 2020

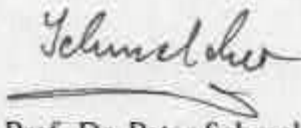
Supervisor: Prof. Dr. Peter Schmelcher

© Kush Mohan Mittal 2020

All rights reserved

Certificate

This is to certify that this dissertation entitled "Correlation effects in the Magnetic properties and nonequilibrium quantum dynamics of spinor Bose Einstein Condensates" towards the partial fulfilment of the BS-MS dual degree programme at the Indian Institute of Science Education and Research, Pune represents study/work carried out by Kush Mohan Mittal at Institute for Laserphysics, University of Hamburg under the supervision of Prof. Dr. Peter Schmelcher, Professor, Institute for Laserphysics, University of Hamburg, during the academic year 2019-2020.



Prof. Dr. Peter Schmelcher



Kush Mohan Mittal

Committee:

Prof. Dr. Peter Schmelcher

Dr. M. S. Santhanam

To,

Mom for being my first teacher.

Dad for sacrificing his M.Sc, for I could complete mine.

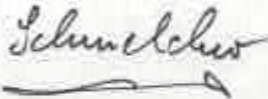
Sister for always being there.

“Yesterday is history, tomorrow is a mystery, but today is a gift.
That’s why we call it the present.”

— Bill Keane

Declaration

Thereby declare that the matter embodied in the report entitled "Correlation effects in the Magnetic properties and nonequilibrium quantum dynamics of spinor Bose Einstein Condensates", is the result of the work carried out by me at the Institute for Laserphysics, University of Hamburg, Indian Institute of Science Education and Research, Pune, under the supervision of Prof. Dr. Peter Schmelcher and the same has not been submitted elsewhere for any other degree.



Prof. Dr. Peter Schmelcher



Kush Mohan Mittal

Acknowledgment

I would like to express my sincere thanks to Prof. Dr. P. Schmelcher, Dr. S.I. Mistakidis and G.M. Koutentakis for their constant motivation during my thesis. Through them, I learned various values that I shall remember throughout my life. I would also like to thank Dr. M. S. Santhanam for being part of my thesis advisory committee and his constant guidance throughout my degree. Further, I am grateful for the teaching and support of Dr. G.J.Sreejith, Dr. Denis Ullmo, and Dr. Olivier Giraud during my degree.

I thank my family for all their love and support without whom this journey would have been impossible. I would further like to express my eternal love to my friends for making this degree an adventure that I shall cherish for my lifetime. The boundaries of this thesis fall short to express my affection for the IISER Pune community, but on a closing note, 'For you all, a thousand times over'.

The financial support through the INSPIRE Fellowship, CNRS research internship and the University of Hamburg is acknowledged.

Permission

This thesis is based on the following work which is expected to be published in the near future:

- Kush Mohan Mittal, S. I. Mistakidis, P. G. Kevrekidis, and P. Schmelcher. Many-body effects on second-order phase transition in spinor Bose-Einstein condensates and breathing dynamics. arXiv:2004.09303

Abstract

We explore the changes in the phase diagram of spin-1 Bose gas due to incorporation of correlations and the finite size of the system. We find that the correlations lead to a significant shift in the phase-boundaries referring to second order phase transitions and this effects becomes further amplified when the number of particles decreases. Further, we study the response of various initial conditions corresponding to different phases after a sudden quench in the optical trap frequency in both within and beyond the mean field limit. We find that irrespective of the initial state there is an induced breathing motion of a same frequency which is also equal for all spin states in either limit. Additionally, the incorporation of correlations lead to the formation of filament like structures. Moreover, for the Broken axisymmetry phase, characterized by occupation of all spin states, we even notice spin flip dynamics. To further quantify the effect of correlations we also study the corresponding one-body and two-body correlation function. Finally, we also find that these filaments like structure become more prominent when one decreases the particle number or increases the spin-independent interaction strength of the system.

Contents

Abstract	xv
1 Introduction	1
2 Methodology	5
3 Results and Discussion	9
3.1 Phase Space Analysis	9
3.2 Quench Dynamics	17
4 Conclusions and Outlook	25
5 Appendix	27
5.1 Natural Population	27
5.2 Quench analysis	30

Chapter 1

Introduction

Since the first realisation of an optically trapped Bose-Einstein condensate with spin degree of freedom in ^{23}Na atoms [1], these systems have been among the most actively studied topics within the ultracold quantum gases community [2–5]. The rich phase diagram emanating within these systems [6–9] render them particularly important for understanding quantum phase transitions. Another interesting consequence of the spin degree of freedom is the presence of spin dynamics in these systems through spin-exchange collision. This involves coherent and reversible transfer of atoms between the magnetic sublevels of the system while conserving their total spin. Such spin dynamics have been confirmed in spin-1 ^{87}Rb [10] and ^{23}Na [6], spin-2 ^{87}Rb [11, 12] as well as spin-3 ^{52}Cr [13].

Considering the rich physics associated with spinor Bose gas, they have been subjected to extensive research. Notable examples include, interferometry applications [14, 15], entanglement studies [16, 17], formation of spin domains and spin textures [18–20], realising soliton complexes [21–25] and the study of universality in spin-dynamic [26–28], however such studies mainly rely on the mean field approximation. Such widespread applications of these system motivates us to study their ground state, as well as, dynamical behavior in the case that correlations are properly accounted for.

The rich phase space structure of spinor Bose gas has been a topic of active research [29–31]. These studies include, decay to ground state of spin-1 Bose gas through quantum tunneling [32], the study of the phase diagram for a spin-2 Bose gas using spin exchange dynamics [33], as well as, induction of phase separation like phenomena in spin-3 Bose gas [34]. Motivated by the rich

phase space structure of these systems, we unravel the alteration of the phase space properties and quench dynamics due to the influence of correlation effects for spin-1 Bose gas by systematically comparing the structures emanating within and beyond the mean field approximation. Further, we also explore the changes in the phase space because of the finite size of the system. We observe that even though there is no noticeable change in the first order transitions, the second order transitions are significantly altered when the correlations are taken into account. The transition boundary for second order transitions is considerably shifted for both ferromagnetic and anti-ferromagnetic interactions. Moreover, we find that the finite size of the system plays a vital role as the alterations because of correlations being more prominent for decreasing particle number.

The presence of multiple phases and the spin dynamics make such systems interesting ground for quench studies [35–39]. Here, we quench the trapping frequency of spin-1 Bose gas system. We study how particles in different phase space state respond to the quench, as well as, how this behavior changes with change in particle numbers and interaction strength, both within and beyond the mean field approximation. In particular, we observe that the quench induces breathing motion [40–42] into the system. Interestingly, the different spin states have same period of oscillation and even spin fluctuations [43] are present for a particular initial phase space state. Additionally, we observe that incorporation of correlations lead to formation of filament [42, 44] like structure in the density profile of the system which become more prominent with a decrease in the number of particles, as well as, an increase in the interaction strength. To quantify the effect of correlations, we further employ the one-body and two-body correlation function. We find that a particle within the filaments are coherent while between neighbouring filaments we have loss of coherence. Moreover, we find that two particles within the filaments are anti correlated while particles between neighbouring filaments are correlated to each other. Further, we see how the changes in filaments number and structure due to a change in interaction strength and particle number shows up in two body correlation function.

Our system comprises of interacting Spin-1 Bose gas of mass M trapped in a 1D harmonic trap and we aim to investigate the system in mean field as well as beyond the mean field regime. The many body (MB) Hamiltonian of such a system can be written as the sum $\hat{H} = \hat{H}_0 + \hat{V}$, where the non interacting part of the Hamiltonian \hat{H}_0 is

$$\hat{H}_0 = \int dx \sum_{\alpha, \beta = -1}^1 \hat{\psi}_\alpha^\dagger(x) \left[-\frac{\hbar^2}{2M} \left(\frac{d}{dx} \right)^2 + \frac{1}{2} M \omega^2 x^2 - p(f_z)_{\alpha\beta} + q(f_z^2)_{\alpha\beta} \right] \hat{\psi}_\beta(x), \quad (1.1)$$

here $\hat{\psi}_\alpha(x)$ denotes the bosonic field operator with spin $\alpha = -1, 0, 1$, ω is the trapping frequency and f_z corresponds to the z-component of the spin matrix whose elements are $(f_z)_{mm'} = m\delta_{mm'}$. Here $p = -g\mu_B B$ is the linear zeeman where g is the Landé hyperfine g-factor, $\mu_B = e\hbar/2m_e$ ($e > 0$ is the charge, m_e is the electron mass) is the Bohr magneton and B is the external magnetic field which is applied in z direction. While, q is the quadratic zeeman term which has contributions from the external field (q_B) and the microwave field (q_{MW}), tuned independent of each other. Considering the system is extremely dilute we consider only the binary interactions for the interacting part of the Hamiltonian which is given by

$$\hat{V} = \frac{1}{2} \int dx \left[c_0 : \hat{n}^2(x) : + c_1 : \hat{F}^2(x) : \right]. \quad (1.2)$$

Here $: :$ denotes normal ordering which leads to the annihilation operators being placed to the right of creation ones. The interaction parameters are expressed as

$$c_0 = \frac{4\pi(a_0 + 2a_2)}{3a_\perp} \quad \text{and} \quad c_1 = \frac{4\pi(a_0 - a_2)}{3a_\perp} \quad (1.3)$$

where a_0 and a_2 are the three dimensional s-wave scattering lengths of the atoms in scattering channels with the total spin $F=0$ and $F=2$ [45]. Here, c_1 can be tuned by using the microwave-induced Feshbach resonance [46]. While, the total-spin operator reads

$$: \hat{F}^2 := \int dx \int dy \sum_{\alpha, \beta, \gamma, \delta = -1}^1 \left[\sum_{i \in \{x, y, z\}} (f_i)_{\alpha\beta} (f_i)_{\gamma\delta} \right] \hat{\psi}_\alpha^\dagger(x) \hat{\psi}_\gamma^\dagger(y) \hat{\psi}_\delta(y) \hat{\psi}_\beta(x). \quad (1.4)$$

Finally, $a_\perp = \sqrt{\hbar/(M\omega_\perp)}$ is the transverse confinement length and ω_\perp the corresponding trapping frequency. As the total density operator $\hat{n}(x)$ reads

$$\hat{n}(x) = \sum_{\alpha = -1}^1 \hat{\psi}_\alpha^\dagger(x) \hat{\psi}_\alpha(x), \quad (1.5)$$

the normal ordered $n^2(x)$ in Eq.(1.2), expressed in terms of field operator becomes

$$: \hat{n}^2(x) := \sum_{\alpha, \beta = -1}^1 \hat{\psi}_\alpha^\dagger(x) \hat{\psi}_\beta^\dagger(x) \hat{\psi}_\beta(x) \hat{\psi}_\alpha(x). \quad (1.6)$$

While the spin density operator $\hat{F}_i(x)$ posses the form

$$\hat{F}_i(x) = \sum_{\alpha, \beta=-1}^1 (f_i)_{\alpha\beta} \psi_{\alpha}^{\dagger}(x) \psi_{\beta}(x). \quad (1.7)$$

where $i \in \{x.y.z\}$, $(f_x)_{\alpha\beta} = \delta_{\alpha, \beta+1} + \delta_{\alpha, \beta-1}$ and $(f_y)_{\alpha\beta} = -i\delta_{\alpha, \beta+1} + i\delta_{\alpha, \beta-1}$. This leads to the normal ordered $\hat{F}^2(x)$ in Eq.(1.2) become

$$:\hat{F}^2(x): = \sum_{\alpha, \beta, \gamma, \delta=-1}^1 \left[\sum_{i \in \{x,y,z\}} (f_i)_{\alpha\beta} (f_i)_{\gamma\delta} \right] \psi_{\alpha}^{\dagger}(x) \psi_{\gamma}^{\dagger}(x) \psi_{\delta}(x) \psi_{\beta}(x). \quad (1.8)$$

Further, we scale the many-body Hamiltonian in the units of $\hbar\omega_{\perp}$. Following this, the corresponding length, time and interaction strengths are provided in terms of $\sqrt{\frac{\hbar}{m\omega_{\perp}}}$, ω_{\perp}^{-1} and $\sqrt{\frac{\hbar^3\omega_{\perp}}{M}}$ respectively.

As evident from above, spin-1 Bose gas form interesting experimentally realisable system. The possibility to easily tune various parameters experimentally makes them particularly interesting to study. In this work as mentioned, we study both the ground state, as well as, dynamical properties of spin-1 Bose gas. In Chap. 2 we describe our numeric method ML-MCTDHX, this can be used to simulate numerous quantum systems in the few particle limit. In Chap. 3 we present and discuss our results for the phase space analysis, as well as, quench dynamics. In Chap. 4 we give the conclusion and outlook for our work. Finally, in Chap. 5 we provide some additional data to support our results.

Chapter 2

Methodology

Our approach to solve the many body Schrödinger equation $(i\hbar\partial_t - \hat{H}) |\Psi(t)\rangle = 0$ relies on the Multi-layer Multi-Configuration Time-Dependent Hartree method for atomic Mixtures [47, 48] (ML-MCTDHX). ML-MCTDHX is an ab-initio variational method for solving the time-dependent MB Schrödinger equation of atomic mixtures consisting of Bosonic or Fermionic species. The key idea of ML-MCTDHX lies in the usage of a time-dependent and variationally optimized MB basis set, that allows for the optimal truncation of the total Hilbert space. This enables us to capture the important correlation effects in a computationally feasible manner. Together, the moving variationally optimised basis set coupled with the multi-layer nature of the ansatz, enables the adaptation of ML-MCTDHX to a system specific method, with increased computational efficiency.

The ansatz for our MB wavefunction, $|\Psi(t)\rangle$, is taken as a linear combination of time-dependent permanents $|\vec{n}(t)\rangle$, with time-dependent weight coefficients $A_{\vec{n}}(t)$

$$|\Psi(t)\rangle = \sum_{\vec{n}} A_{\vec{n}}(t) |\vec{n}(t)\rangle. \quad (2.1)$$

Each time-dependent permanent is expanded in terms of M time-dependent variationally optimized single-particle spin-orbitals (SPSOs) $\Phi_j(x, \alpha; t)$, $\alpha = +1, 0, -1$, $j = 1, 2, \dots, M$ with occupation numbers $\vec{n} = (n_1, \dots, n_M)$. Subsequently, the SPSOs are expanded in a basis spanned by m distinct time-dependent single-particle functions (SPFs) $\{\phi_k(x; t)\}$ possessing information only on the spatial state of the particle, and are independent on the three-dimensional basis for the $S = 1$ degree

of freedom $\{|+1\rangle, |0\rangle, |-1\rangle\}$. Therefore the SPSO read

$$\Phi_j(x, \alpha; t) = \sum_{k=1}^m B_{k\alpha}^j(t) \phi_k(x; t), \quad (2.2)$$

where $B_{k\alpha}^j(t)$ refer to the corresponding time-dependent expansion coefficients. Finally, each $\phi_k(x; t)$ is discretized in terms of a discrete variable representation (DVR). The time-evolution of the N -body wavefunction under the effect of the Hamiltonian \hat{H} reduces to the determination of the A -vector coefficients, the $B_{k\alpha}^j(t)$ expansion coefficients for the SPSOs and the SPFs, which in turn follow the variationally obtained ML-MCTDHX equations of motion [47, 48]. The latter consists of a set of $\binom{N+M-1}{M-1}$ ordinary linear differential equations for the A -vector coefficients, coupled to M and m non-linear integrodifferential equations for the SPSOs and SPFs respectively. In the limiting case of $M = 1$ and $m = 3$, the method reduces to the time-dependent Gross-Pitaevskii equation for a three-component system. Indeed within this limit only a single SPSO is involved as the MB ansatz is given by $\phi(x_1, \alpha_1, x_2, \alpha_2, \dots, x_n, \alpha_n) = \prod_{i=1}^N \Phi_1(x_i, \alpha_i, t)$. The corresponding equation of motion for spin +1 and spin -1 is

$$\begin{aligned} i\partial_t \Phi_1(x, \pm 1; t) = & \left(-\frac{1}{2} \frac{d^2}{dx^2} + \frac{1}{2} \omega^2 x^2 - p \pm q \right) \Phi_1(x, \pm 1; t) + c_0 \sum_{\alpha=-1}^1 |\Phi_1(x, \alpha; t)|^2 \Phi_1(x, \pm 1; t) \\ & + c_1 (|\Phi_1(x, \pm 1; t)|^2 + |\Phi_1(x, 0; t)|^2 - |\Phi_1(x, \mp 1; t)|^2) \Phi_1(x, \pm 1; t) + c_1 |\Phi_1(x, 0; t)|^2 \Phi_1^*(x, \mp 1; t), \end{aligned} \quad (2.3)$$

and for the spin 0 reads

$$\begin{aligned} i\partial_t \Phi_1(x, 0; t) = & \left(-\frac{1}{2} \frac{d^2}{dx^2} + \frac{1}{2} \omega^2 x^2 \right) \Phi_1(x, 0; t) + c_0 \sum_{\alpha=-1}^1 |\Phi_1(x, \alpha; t)|^2 \Phi_1(x, 0; t) + c_1 (|\Phi_1(x, +1; t)|^2 \\ & + |\Phi_1(x, -1; t)|^2) \Phi_1(x, 0; t) + 2c_1 \Phi_1(x, +1; t) \Phi_1^*(x, 0; t) \Phi_1(x, -1; t). \end{aligned} \quad (2.4)$$

In the case of $M = 3M_p$, $m = M_p$, where M_p is the dimension of the DVR basis, the ML-MCTDHX method is equivalent to a full configuration interaction approach (commonly referred to as “exact diagonalization” in the literature).

For our implementation we have used a sine DVR as a primitive basis for the spatial part of the SPFs. Note that the sine-DVR inherently introduces hard-wall boundary conditions at its endpoints. In particular we have employed $x_{\pm} = \pm 40$ for $N = 50$ particles, $x_{\pm} = \pm 35$ for $N =$

20 particles and $x_{\pm} = \pm 25$ for $N = 5$ particles. We have ensured while choosing these boundary points that their location is such that it does not affect our results. To study the dynamics, we propagate the wavefunction by utilizing the appropriate Hamiltonian within the ML-MCTDHX equations of motion. To verify the accuracy of the numerical integration, we impose the following overlap criteria $|\langle \Psi(t) | \Psi(t) \rangle - 1| < 10^{-8}$ for the total wavefunction and $|\langle \Phi_i | \Phi_j \rangle - \delta_{ij}| < 10^{-9}$, $|\langle \phi_i | \phi_j \rangle - \delta_{ij}| < 10^{-9}$ for the SPSOs and SPFs respectively. In addition, the accuracy of the ML-MCTDHX approach has been verified by calculating the behaviour of the system for different values of M and m . More specifically, in the following we employ $M = 4$, $m = 6$ for the $N = 50$ case, $M = 6$, $m = 6$ for the $N = 20$ case and $M = 6$, $m = 6$ for the $N = 5$ case.

Further, for our simulations we fix the value of $c_0 = 1$, while the experimentally realisable value $c_1 = 0.018 \sqrt{\hbar^3 \omega_{\perp} / M}$, corresponding to the interaction between ^{23}Na atoms, is taken for exploring the an anti-ferromagnetic $c_1 < 0$ condensate. Whereas within ferromagnetic case we consider a value of $c_1 = -0.0047 \sqrt{\hbar^3 \omega_{\perp} / M}$ which corresponds to ^{87}Rb atoms.

We further show in Appendix that there is substantial occupation for orbitals corresponding to the beyond mean field limit for the phase space, as well as, the quench studies. This occupation leads to very interesting physics which we shall report below.

Chapter 3

Results and Discussion

3.1 Phase Space Analysis

The interplay between the sign of c_1 and various values of p, q results in a rich phase space diagram in the thermodynamic limit, when the mixing between the spatial and spin degrees of freedom of the spin-1 Bose gas are ignored, see Fig. 3.1. When considering anti-ferromagnetic interactions $c_1 > 0$, there are two ferromagnetic phases with particles residing either in the $f_z = +1$ (F1) or the $f_z = -1$ (F2) state. Moreover, there is an anti-ferromagnetic phase (AF), in which the particles are present in both the $f_z = +1$ and the $f_z = -1$ state while the $f_z = 0$ state remains unoccupied. Also, there is the Polar phase (P) which comprises of particles being entirely in the $f_z = 0$ state and is involved in the first order transitions. For ferromagnetic interactions namely $c_1 < 0$ one additional phases emerge, the broken-axisymmetry phase (BA) which comprises of all the three spin states being occupied. As is evident, there are numerous quantum phase transitions possible for this system, see Fig. 3.1. These transitions between the various phases, can be classified according to their continuous (second order) or non-continuous (first order) character. The first order transitions are characterized by the abrupt change of the spin-state that contributes to the ground state, as the transition point is crossed. For instance, within the F1 state all of the particles occupy the spin-state $f_z = 1$ while within the P state all particles occupy the state $f_z = 0$. Namely along the curve (see red line in Fig. 3.1(a)) of the F1 to P phase transition the spin-state contributing to the ground state changes from $f_z = 1$ to $f_z = 0$ without accessing a superposition state of the $f_z = 0$ and the $f_z = 1$ components. In contrast, for second order phase transitions the ground state transits from a state

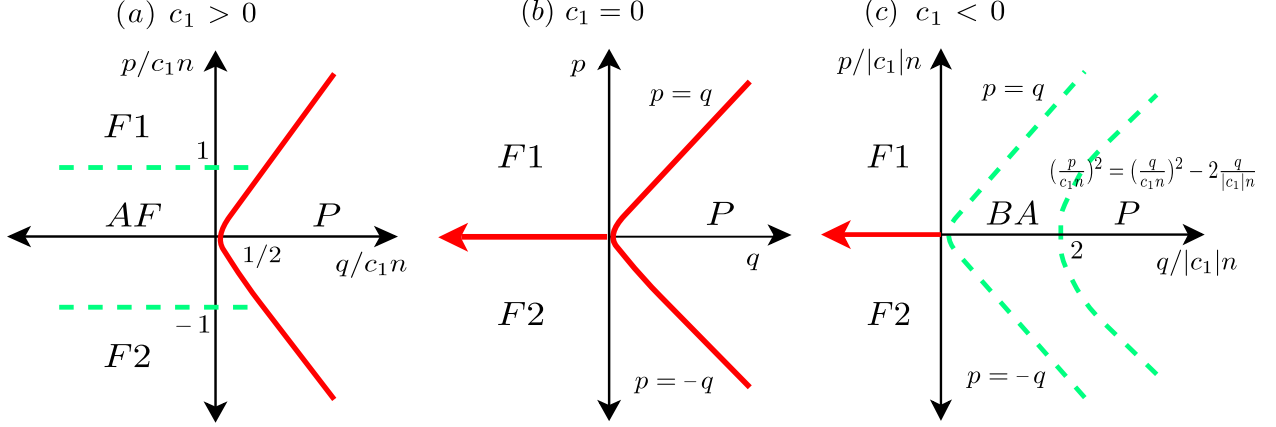


Figure 3.1: Phase diagram of the spin-1 Bose gas for (a) $c_1 > 0$, (b) $c_1 = 0$ and (c) $c_1 < 0$ and varying linear p and quadratic q Zeeman shift parameters in the thermodynamic limit where the hybridization of spin and spatial degrees of freedom is neglected. Red-solid lines denote the first-order phase transition boundaries, while the green-dashed lines denote the second-order phase transition boundaries and n refers to the density of Bose gas. The phase diagram comprises of two ferromagnetic phases (F1, F2), an anti-ferromagnetic phase (AF), a polar phase (P) and a broken asymmetry phase (BA) explained explicitly in the text.

characterized by the occupation of a single-spin state to a superposition one where a second spin-state acquires finite population as the phase boundary is crossed. For instance, along the transition curve from F2 to the AF state (see the green-dashed lines in Fig. 3.1(a)), the system initially occupies $f_z = -1$ state and then resides in a superposition of the $f_z = 1$ and the $f_z = -1$ states. Below, we compare the mean field and beyond mean field phase structure of a spin-1 Bose gas and explore the effect of the finite size of the system on the respective phase diagram. Hereby we focus on the continuous phase transitions, and explore their alterations due to finite particle number and the presence of correlations. Indeed, the emergence of correlations when beyond mean field effects are considered leads to a substantial change in the phase structure corresponding to second order transitions as we shall show explicitly below. We remark that the impact of correlations has also been explored across the corresponding first order transitions and it has been found that their inclusion does not lead to a substantial change of their boundaries. See for instance Fig. 3.2 where we shown the $\langle \hat{F}_z \rangle$ and $\langle \hat{P} \rangle$ for the transition from F2 to P to F1 for increasing p and constant $q = 0.5$ where the interaction is given by $c_1 = 0$.

In particular for anti-ferromagnetic interactions $c_1 > 0$, we focus on the second order phase transitions which are known to occur in the $q < 0$ region and involve the phases F1, F2 and AF, see Fig. 3.1(a). For all of these phases we expect the $f_z = 0$ state to be unoccupied. To explicitly

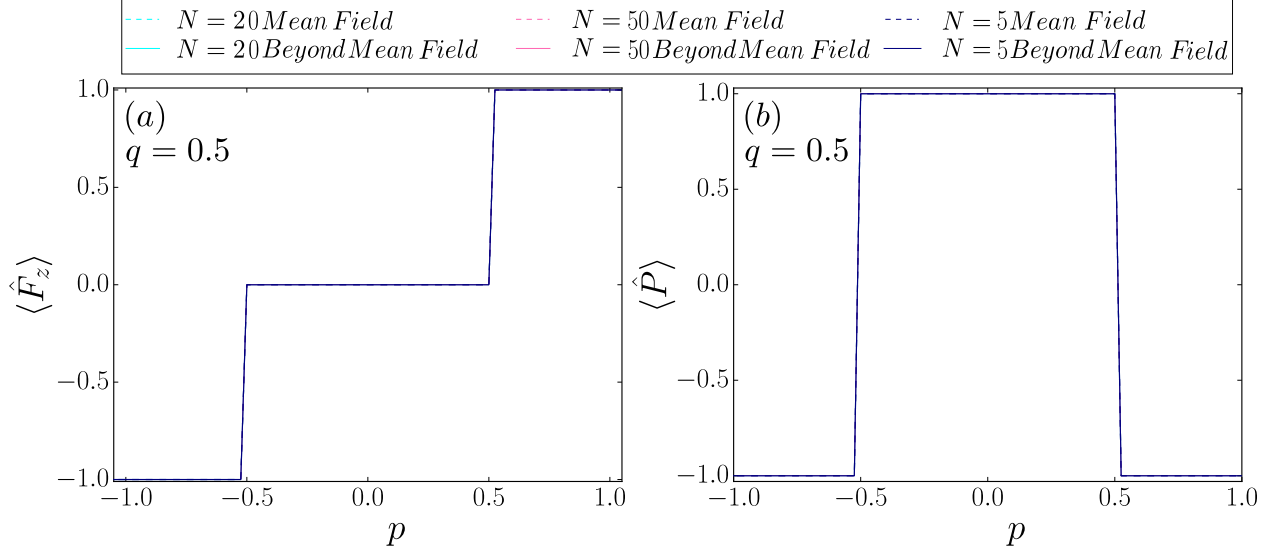


Figure 3.2: (a) corresponds to $\langle \hat{F}_z \rangle$ for the first order transitions both within and beyond the mean field approximation and different N (see legend). The transitions is among the F2, P and F1 phases for increasing p , constant $q = 0.5$ and $c_1 = 0$. While, (b) shows $\langle \hat{P} \rangle$ for the same transition. Note, as the lines are overlapping they can't be differentiated in the figure.

demonstrate that the $f_z = 0$ state remains unoccupied throughout this transition we employ the “polar state operator” that reads

$$\hat{P} = \sum_{\alpha\beta} \int \hat{\psi}_{\alpha}^{\dagger}(x) P_{\alpha\beta}^o \hat{\psi}_{\beta}(x) dx = \hat{n}_o - (\hat{n}_1 + \hat{n}_{-1}).$$

Here $P_{\alpha\beta}^o = (1 - 2|\alpha|)\delta_{\alpha\beta}$, with $\alpha, \beta \in \{-1, 0, 1\}$ and \hat{n}_i corresponds to the number operator of the i^{th} spin state. The expectation value of the polar-state operator $\langle \hat{P} \rangle$, quantifies the difference between the number of particles in the $f_z = 0$ state to that of the ones in the $f_z = \pm 1$ state. Thus, for the above-mentioned phases i.e, F1, F2 and AF, one expects the $\langle \hat{P} \rangle = -1$ which is verified in Fig. 3.5(a) both within the mean field, as well as, in the beyond mean field case. In order to examine the phase transitions between the above described phases, we further employ as an order parameter the expectation value of the spin-z operator

$$\hat{F}_z = \sum_{\alpha\beta} \int \hat{\psi}_{\alpha}^{\dagger}(x) (f_z)_{\alpha\beta} \hat{\psi}_{\beta}(x) dx = \hat{n}_1 - \hat{n}_{-1}. \quad (3.1)$$

Accordingly, $\langle \hat{F}_z \rangle = 1$ and $\langle \hat{F}_z \rangle = -1$ indicate the F1 and the F2 phase respectively while if $-1 < \langle \hat{F}_z \rangle < 1$ then the AF phase for $c_1 > 0$ interaction. The transition comprises of the sys-

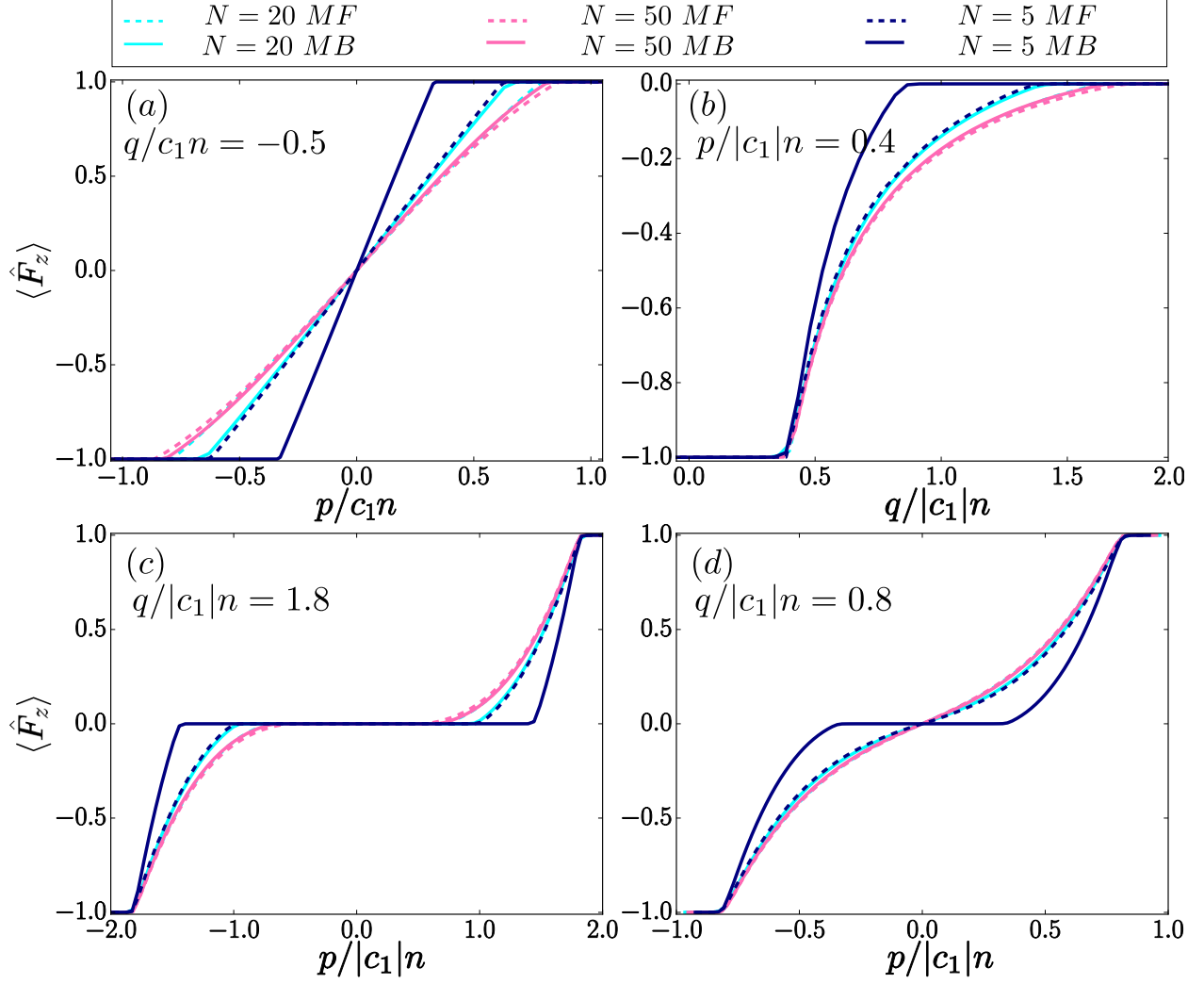


Figure 3.3: $\langle \hat{F}_z \rangle$ for the second order transitions both within and beyond the mean field approximation and different N (see legend). (a) corresponds to the transitions among the F2, AF and F1 phases for increasing $p/c_1 n$, constant $q/c_1 n$ and $c_1 > 0$. While, $\langle \hat{F}_z \rangle$ for ferromagnetic interactions ($c_1 < 0$) and transitions (b) among F2, BA and P for increasing $q/|c_1|n$ and constant $p/|c_1|n$, (c) among F2, BA, P, BA and F1 and (d) among F2, BA and F1 for increasing $p/|c_1|n$ and constant $q/|c_1|n$.

tem transforming continuously from F2 to the F1 state via the AF state as $p/c_1 n$ is increased for a fixed negative $q/c_1 n$. Note that here $n = \sum_{\alpha} \langle \psi_{\alpha}^{\dagger}(x=0) \psi_{\alpha}(x=0) \rangle$ is the total density at the trap centre in the mean field. Our results regarding $\langle \hat{F}_z \rangle$ are presented in Fig. 3.3(a). We find that the range of $p/c_1 n$ values where the AF state is accessed decreases when the correlations are included, as the point of transition is shifted towards $p/c_1 n = 0$ in the latter case, compare in particular the MF and MB results for $N = 5, 20$ and 50 particles in Fig. 3.3(a). Note that within the AF phase

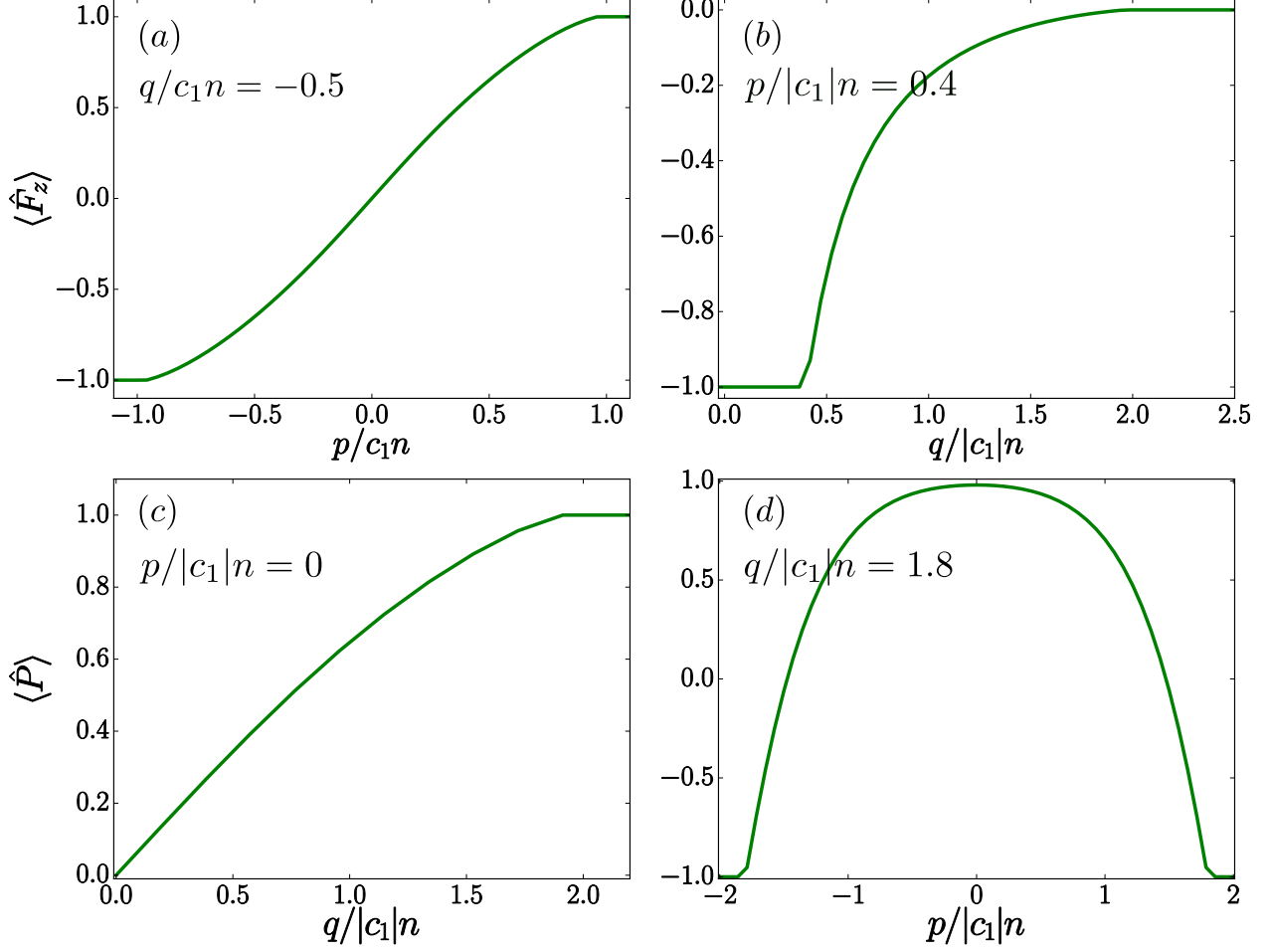


Figure 3.4: Second order transitions in the mean field approximation and $N = 500$ particles. (a) corresponds to $\langle \hat{F}_z \rangle$ for the transition among the F1, AF and F2 phases for increasing $p/c_1 n$, constant $q/c_1 n = -0.5$ and $c_1 > 0$. While, $\langle \hat{F}_z \rangle$ for ferromagnetic interactions ($c_1 < 0$) and transitions among F2, BA and P for increasing $q/|c_1|n$ and constant $p/|c_1|n = 0.4$ is shown in (b), (c) shows $\langle \hat{P} \rangle$ for $c_1 < 0$ and the transition P, BA and F1 occurring at fixed $p/|c_1|n = 0$ and increasing $q/c_1 n$, (d) among F2, BA and F1 for increasing $p/|c_1|n$ as $q/|c_1|n = 1.8$ is constant for $c_1 < 0$.

$\langle \hat{F}_z \rangle$ increases roughly linearly with p . Furthermore, we observe that the transition threshold in terms of $p/c_1 n$, also, decreases as the particle number decreases (compare the case of $N = 5$ to the $N = 20, 50$ particles). As depicted in Fig. 3.1, the phase space transition boundary is known to occur at $p/c_1 n = \pm 1$ [4] but due to the finite size effects emanating in our system, the transition occurs for $p/c_1 n < 1$, see for instance that for $N = 5$ particle in Fig. 3.3(a), here the transition takes place at $p/c_1 n = 0.6$ in the MF limit. To confirm the presence of these finite size effects, we have simulated the behavior of $N = 500$ bosons within the mean field approximation for varying $p/c_1 n$, see Fig. 3.4(a). In this case the transition indeed, occurs for $p/c_1 n \approx 1$.

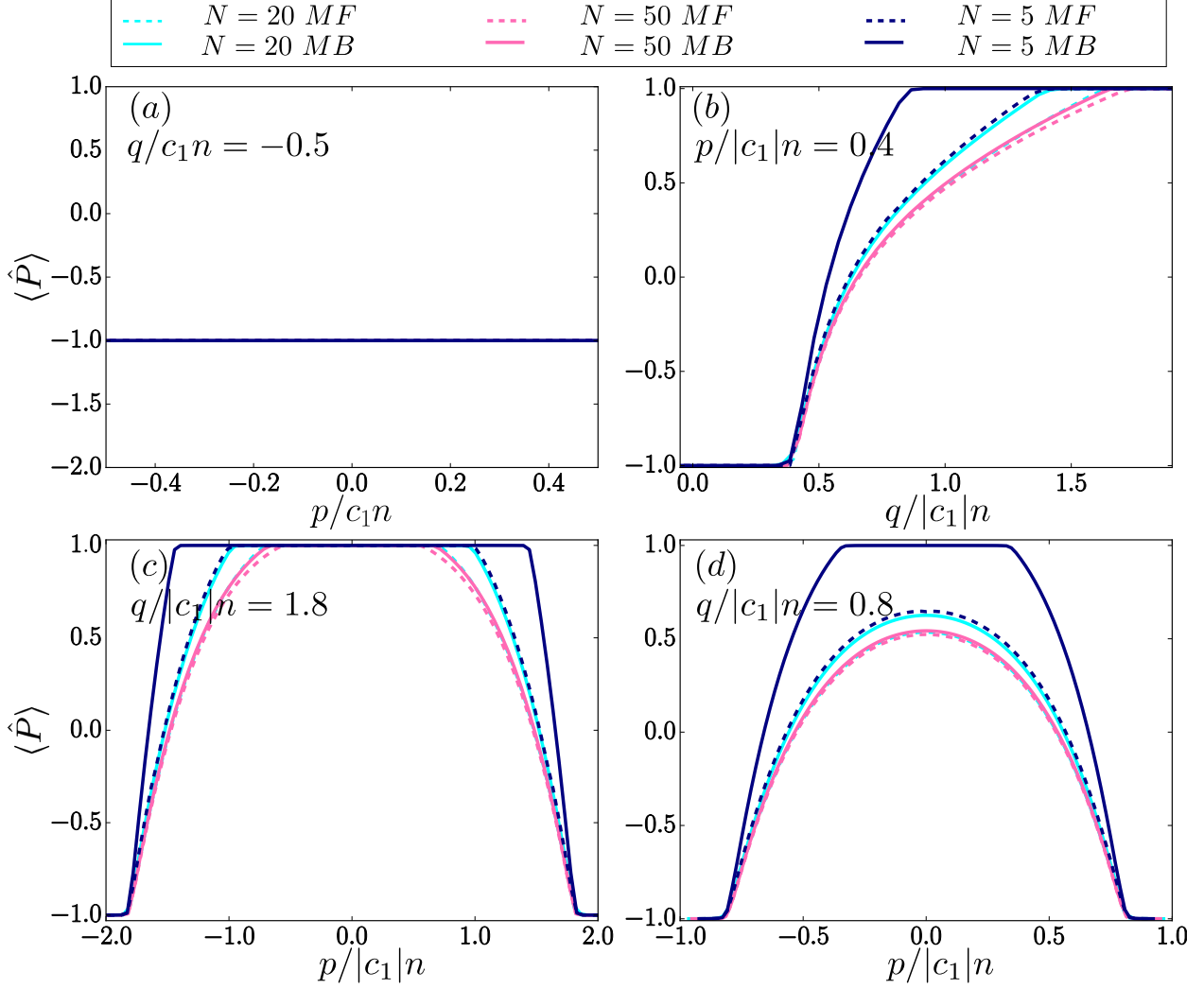


Figure 3.5: $\langle \hat{P} \rangle$ for the second order transitions both within and beyond the mean field approximation and different N (see legend). (a) corresponds to the transition among the F1, AF and F2 phases for increasing $q/c_1 n$, constant $q/c_1 n = -0.5$ and $c_1 > 0$. While, $\langle \hat{P} \rangle$ for ferromagnetic interactions ($c_1 < 0$) and transitions (b) among F2, BA and P for increasing $q/|c_1|n$ and constant $p/|c_1|n = 0.4$, (c) among F2, BA, P, BA and F1 and (d) among F2, BA and F1 for increasing $p/|c_1|n$ as $q/|c_1|n$ is constant.

For the ferromagnetic interactions $c_1 < 0$ there are three distinct second order phase transitions, see Fig. 3.1(c). The involved phases corresponds to the F1 and F2, as well as P and BA phases. Since the Polar phase (P) comprises of particles being entirely in the $f_z = 0$ component, here $\langle \hat{P} \rangle = 1$. While, the broken-axisymmetry phase (BA) comprises of all the three spin states being occupied and refers to $\langle \hat{P} \rangle \in (-1, 1)$. Fig. 3.3(b) shows $\langle \hat{F}_z \rangle$ for fixed $p/|c_1|n = -0.4$ and increasing $q/|c_1|n$. Here, the transition from a state within F2 to a P one via a monotonous increase of $\langle \hat{F}_z \rangle$ through

the BA phase is observed. The phase transition between the F2 and BA phases is expected at $p = -q$ [4]. Indeed our simulations verify this, both within the mean field and the beyond mean field level, as well as, for different particle numbers [Fig. 3.3(b)]. The phase transition from BA to P exhibits a similar behavior to the phase transition in the anti-ferromagnetic $c_1 > 0$ case [Fig. 3.3(a)], with the transition point shifting towards lower q values and the effect being more prominent as the particle number decreases upon including correlations, compare the MF and MB limit for $N = 5, 20$ and 50 particles in Fig. 3.3(b). Due to the non-zero occupation of the $f_z = 0$ state this behaviour is also imprinted in $\langle \hat{P} \rangle$, see Fig. 3.5(b). Furthermore, we note that one expects the transition from BA to P phase to occur at $q/|c_1|n = 2.07$ in the thermodynamic limit [4], see also the behavior of this transition boundary in Fig. 3.1(c). This is not observed in our system owing to its finite size effects. To confirm this, we calculate the behavior of $N = 500$ particles in mean field limit, see the inset of Fig. 3.4(b). Indeed one finds that for $N = 500$ particles, this transition occurs for $q/|c_1|n \approx 2.07$, thus confirming that the above-mentioned behavior is indeed a finite size effect.

Fig. 3.3(c), illustrates $\langle \hat{F}_z \rangle$ for the phase transitions taking place for fixed $q/|c_1|n = 1.8$, varying $p/|c_1|n$ and a ferromagnetically interacting $c_1 < 0$ Bose gas. In this case several phase transitions are expected in the thermodynamic limit as the system transits from F1 to BA and finally to P with $\langle \hat{F}_z \rangle$ monotonously decreasing for decreasing $p > 0$. Additionally, if p further decreases to $p < 0$ the $\langle \hat{F}_z \rangle$ decreases as a result of the transition between P and BA phase, and for even lower p the system eventually transits from the BA to the F2 phase, see $q/|c_1|n > 2$ in Fig. 3.1(c). The transitions between F1 and BA as well as, BA and F2 occur at $p = q$ and $p = -q$ respectively [4], which is unaltered in both the MF and MB case [Fig. 3.3(c)]. Note that in the mean field case and by ignoring the hybridization between the spatial and spin state, one expects that the P state is only accessed for fixed $q/|c_1|n > 2$ [4]. However, in our case the P phase can be accessed for $q/|c_1|n = 1.8$. Indeed, the phase transition boundaries between P and BA shift away from the $p = 0$ when one considers the correlated case and thus the range where the BA phase is accessed is reduced in the latter-case see Fig. 3.5(c). In particular for the $N = 5$ case these transition points occur at $p/|c_1|n = \pm 1.44$ in the MB case compared to $p/|c_1|n = \pm 0.96$ in MF limit. In addition, decreasing the number of bosons also favors the transition towards the P state, compare the case of $N = 5, 20$ and 50 particles in Fig. 3.3(c). Let us remark here, that the behaviour exhibited for decoupled spin and spatial degrees of freedom [4] is realized in the large particle limit of our setup. In particular, we have simulated the MF behavior of $N = 500$ particles for $p/|c_1|n = 0$ and varying q , see Fig. 3.4(c). Here, we observe the transition point to the P state which signifies the onset of transitions as the ones depicted in Fig. 3.5(c) is at $q/|c_1|n \approx 2$ agreeing with the theoretical

predictions of Ref. [4], and thus confirming the presence of finite size effects. To support our arguments, we also show the behavior of $N = 500$ particles for fixed $q/|c_1|n = 1.8$. It becomes evident that the shape of $\langle P \rangle$ agrees with the thermodynamic limit, compare Fig. 3.4(d) and Fig. 3.5(c) with the expected thermodynamic behavior shown in Fig. 3.1(b). The later further assures that this behavior is a finite size effect.

Turning to the second order phase transition from state F2 to F1 through BA for fixed $q/|c_1|n = 0.8$ and $c_1 < 0$, we present $\langle \hat{F}_z \rangle$ for varying $p/|c_1|n$ in Fig. 3.3(d). In the thermodynamic limit phase transitions between the ferromagnetic phases (F1, F2) and BA to occur at $p = q$ and $p = -q$ respectively [4], here $\langle \hat{F}_z \rangle$ decreases monotonously for decreasing $p/|c_1|n$ within the BA phase. In accordance with the above discussed second order transitions [Fig. 3.3(b)-3.3(c)], we see that these phase boundaries indeed occur at $p = \pm q$ and their positions are not significantly altered when correlations are taken into account [Fig. 3.3(d)]. Interestingly, in the correlated case and for $N = 5$ bosons, the transition from the BA to the P state and vice versa is observed for $p/|c_1|n = 0.35$ and $p/|c_1|n = -0.35$ respectively [Fig. 3.3(d) and 3.5(d)]. This effect can be understood due to the fact that the P phase is favorable for smaller values of $q/|c_1|n$ as the particle number decreases when correlation effects are included. For the remaining cases, there are minor changes in the value obtained by $\langle \hat{F}_z \rangle$ within the BA phase occurring between the MB and MF cases, compare the region of BA state between the MB and the MF limit for $N = 20, 50$ particles in Fig. 3.3(d). Similar conclusions can also be drawn by studying the expectation value of $\langle \hat{P} \rangle$, Fig. 3.5(d).

Summarizing, we observe that the area occupied by AF and the BA phases within the phase diagram of a spin-1 Bose gas shrinks for $c_1 > 0$ and $c_1 < 0$ interactions respectively, when one takes correlations into account. Moreover, this effect is more pronounced as the number of particles decreases. Therefore, one can infer that the phases involving a superposition among different spin states are not favourable when one operates beyond the MF approximation and this effect is further amplified by a decrease of the involved particle number.

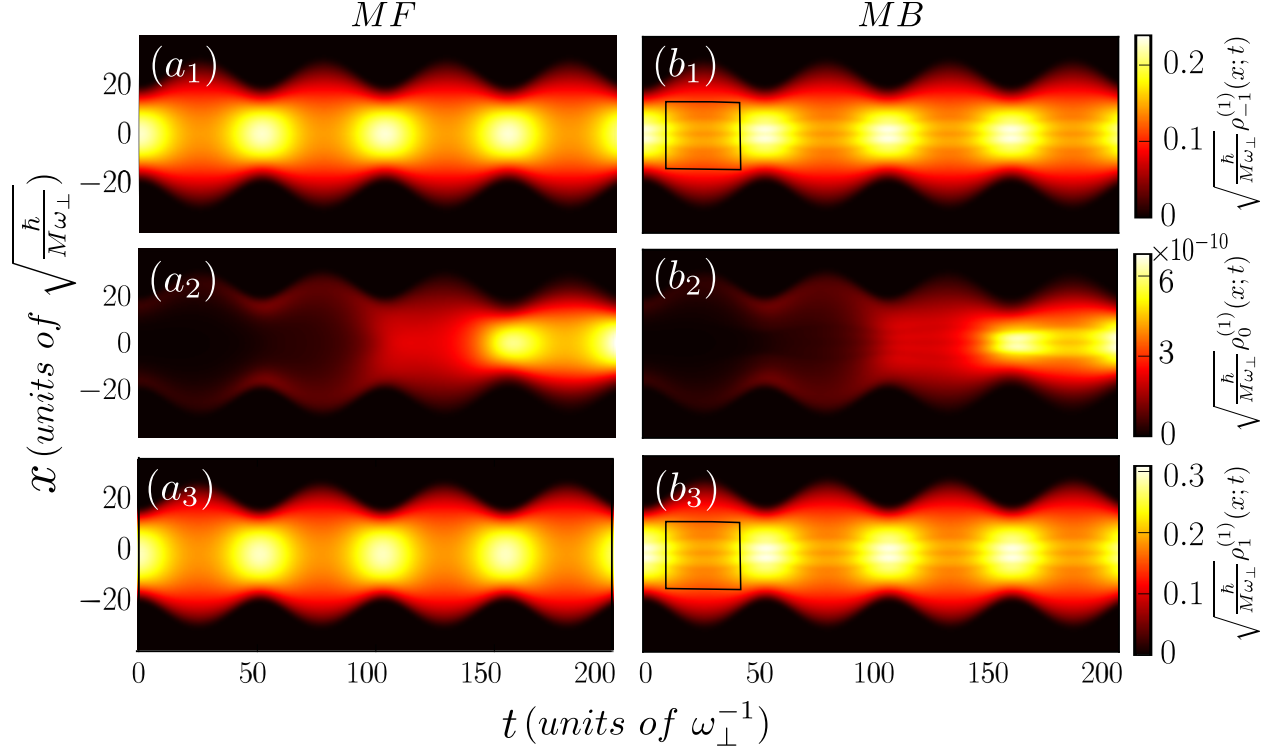


Figure 3.6: Spatiotemporal evolution of the spin-resolved one body densities $\rho_{\sigma}^{(1)}(x;t)$ for the AF state of $N = 50$ particles within (a) mean field and (b) beyond mean field approximation after an abrupt quench of the trapping frequency from $\omega = 0.1$ to $\omega = 0.07$, here $p/c_1n = 0.11$ and $q/c_1n = -0.5$. (a_1, b_1) correspond to $f_z = -1$, (a_2, b_2) correspond to $f_z = 0$ while (a_3, b_3) correspond to $f_z = 1$ state. Note that the color scaling is different for each value of f_z .

3.2 Quench Dynamics

In this section we explore the quench dynamics induced by a sudden decrease of the optical trap frequency for the spin-1 Bose gas consisting of $N = 50$ particles both within and beyond the MF approximation. More specifically, the system is initialized into its ground state in different initial phase space states such as the F1, F2, AF, BA and P states and then an abrupt change of the trapping frequency from $\omega = 0.1$ to $\omega = 0.07$ triggers the dynamics. In Fig. 3.6 the temporal evolution of the one body density $\rho_{\sigma}^{(1)}(x,t) = \langle \psi(t) \psi_{\sigma}^{\dagger}(x) \psi_{\sigma}(x) \psi(t) \rangle$ is demonstrated for a quench within the AF phase, which emanates for antiferromagnetic $c_1 < 0$ spin-spin interactions. This quench results in an induced breathing mode [40, 41] manifested as a contraction and expansion of the atomic cloud around the trap center. Interestingly as can be seen in Fig. 3.6 and Fig. 3.7, the frequency of the oscillation is the same, namely $\omega = 0.12$, for particles in different spin states compare Fig. 3.6(b_1), (b_3), and remains the same for the MF, as well as, the MB case, compare

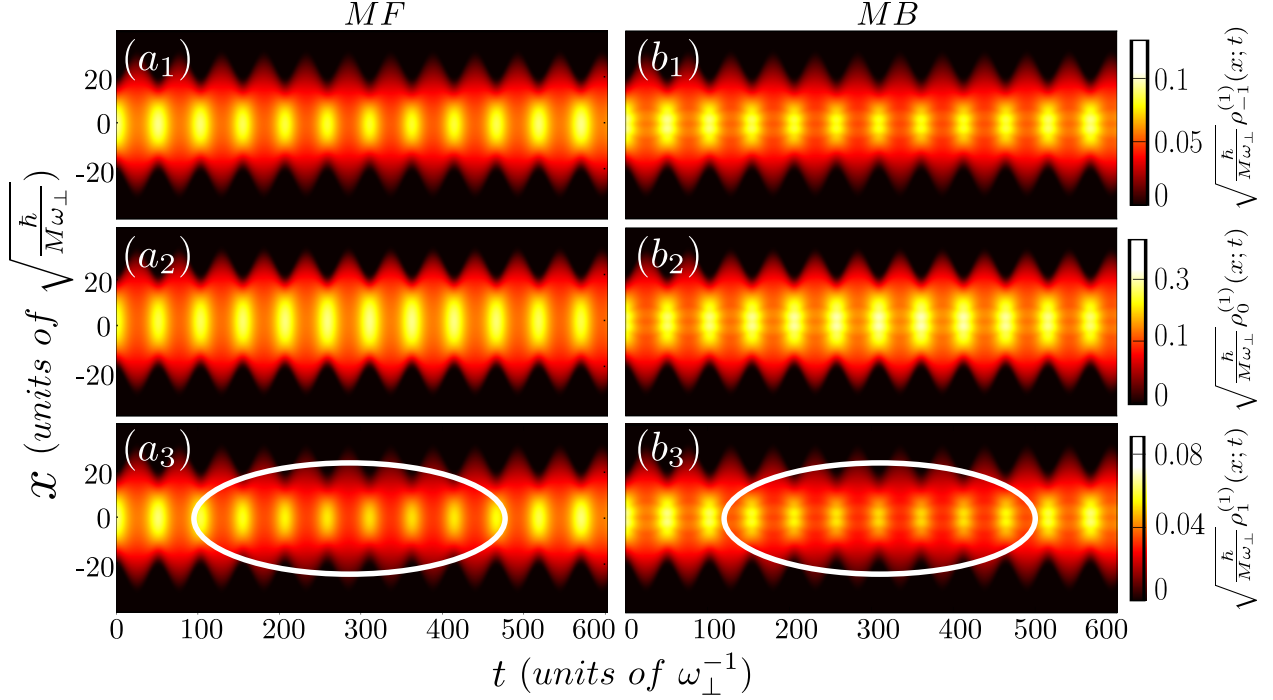


Figure 3.7: Spatiotemporal evolution of the spin-resolved one body densities $\rho_{\sigma}^{(1)}(x;t)$ for the BA state of $N = 50$ particles within (a) mean field and (b) beyond mean field approximation after an abrupt quench of the trapping frequency from $\omega = 0.1$ to $\omega = 0.07$, here $p/|c_1|n = 0.04$ and $q/|c_1|n = -0.44$. (a_1, b_1) correspond to $f_z = -1$, (a_2, b_2) correspond to $f_z = 0$ while (a_3, b_3) correspond to $f_z = 1$ state.

Fig. 3.6(a_1), (b_1). This behaviour is observed irrespective of the initial phase space state subjected to the quench. Additionally, one observes in Fig. 3.6 that the quench of an initially AF state doesn't induce a significant spin flip dynamics as the probability of particles in different spin states remains almost constant with time, while also conserving the spin of the system in the course of evolution. Similar observations can also be made for the initially ferromagnetic (F1, F2) or polar (P) state (see Appendix). Note here that the breathing frequency observed for different initial states referring to distinct phases is almost equal to the previously observed one. Surprisingly, this fact also holds in the case of ferromagnetic spin-spin interactions $c_1 < 0$, see Fig. 3.7 for a system initialised in the BA phase. However in contrast to the above, when an initial state in BA phase is subjected to such a quench a low frequency spin flip dynamics occurs [43], see Fig. 3.7. Here initially the particles in the $f_z = 1$ and the $f_z = -1$ state get transferred coherently to the $f_z = 0$ state while the opposite scenario is subsequently realised, see for instance the region indicated by an ellipse in Fig. 3.7 corresponding to the dynamics of $f_z = 1$. This behavior is also confirmed by the evolution of $\langle \hat{P} \rangle$ during the quench dynamics [Fig. 3.8]. Here $\langle \hat{P} \rangle$ increases initially when

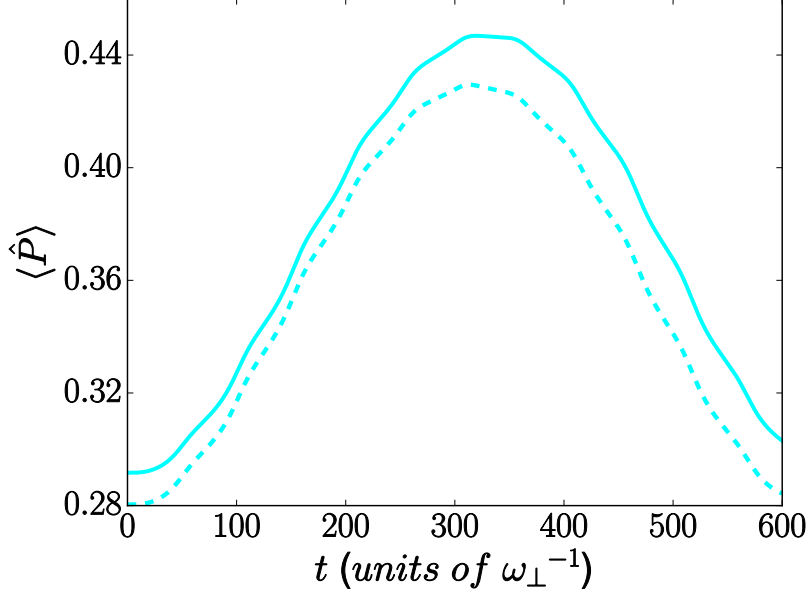


Figure 3.8: $\langle \hat{P} \rangle$ throughout the quench dynamics of an initially BA state shown in Fig. 3.7. Solid line denotes the MB case while the dashed line represents the MF case.

$f_z = \pm 1$ particles get transferred to $f_z = 0$ state and eventually decreases owing to the reverse process. Note also the considerable difference between the Mean field and Beyond Mean field limit in Fig. 3.8. Here $\langle \hat{F}_z \rangle$ remains constant throughout the time-evolution. The most prominent effect of the correlations is the formation of filament like structures building upon the one-body densities of the individual spin-component as depicted in Fig. 3.6 and Fig. 3.7. These filaments are manifested as high particle density structures appearing during the expansion dynamics of the Bose gas, see the box in Fig. 3.6. To explicitly quantify the effect of correlations we employ the normalized one body coherence function

$$g_{\sigma}^{(1)}(x, x'; t) = \frac{\rho_{\sigma}^{(1)}(x, x'; t)}{\sqrt{\rho_{\sigma}^{(1)}(x; t) \rho_{\sigma}^{(1)}(x'; t)}}. \quad (3.2)$$

This observable can be used to measure the proximity of the MB state to a MF (product) state for a fixed set of coordinates x, x' . Here $\rho_{\sigma}^{(1)}(x, x'; t)$ is the one-body reduced density matrix corresponding to the σ component and $\rho_{\sigma}^{(1)}(x; t) = \rho_{\sigma}^{(1)}(x, x' = x; t)$ is the density of the σ component. Additionally, $|g_{\sigma}^{(1)}(x, x'; t)| \in [0, 1]$, with $|g_{\sigma}^{(1)}(x, x'; t)| = 0$ ($|g_{\sigma}^{(1)}(x, x'; t)| = 1$) referring to a fully incoherent (coherent) state. The absence of the imprint of correlations to the coherence function is realised when $|g_{\sigma}^{(1)}(x, x'; t)| = 1$ for every x, x' while the partial incoherence, i.e $|g_{\sigma}^{(1)}(x, x'; t)| < 1$ between two distinct spatial regions signifies the presence of correlations. For the case of $N = 50$

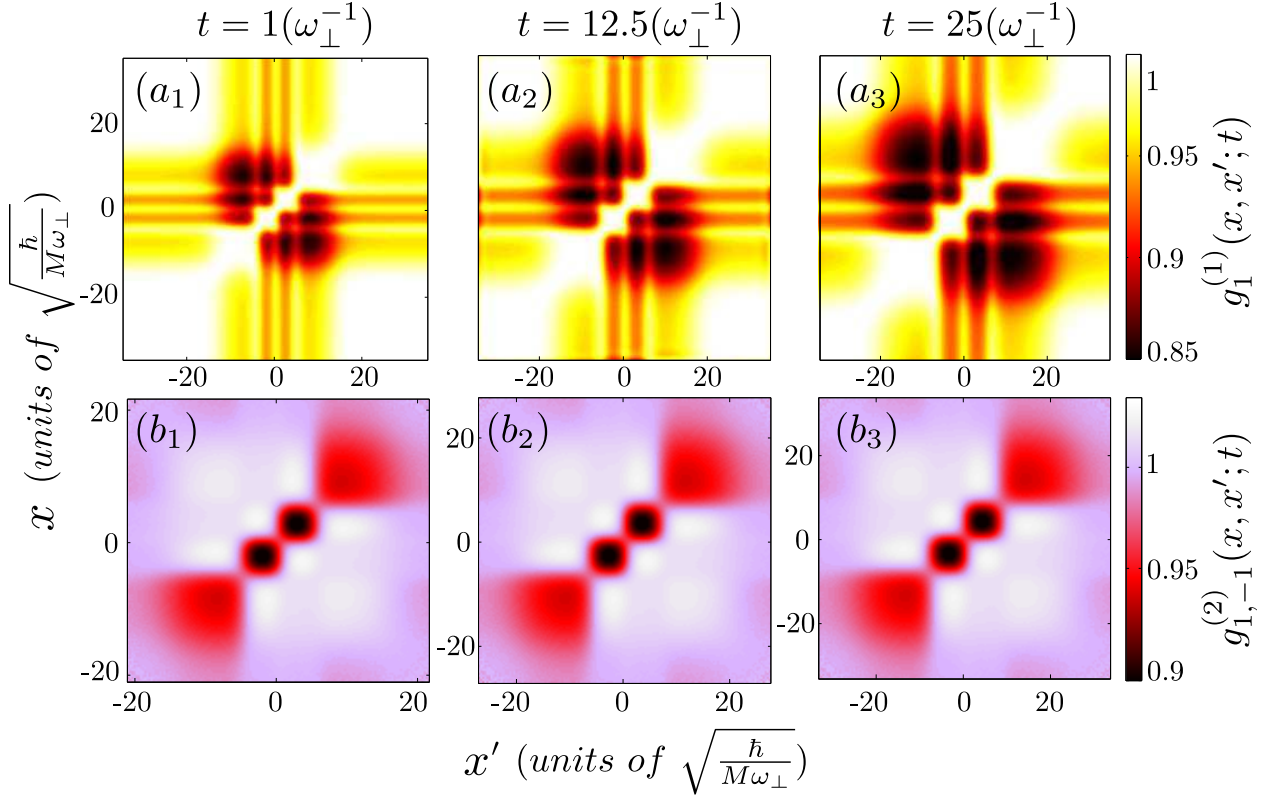


Figure 3.9: $(a_1), (a_2), (a_3)$ are the one body coherence $g_1^{(1)}(x, x'; t)$ and $(b_1), (b_2), (b_3)$ are the two body correlations $g_{1,-1}^{(2)}(x_1, x_2; t)$ for, $(a_1), (b_1)$ $t=1$ (density spread minima), $(a_2), (b_2)$ $t=12.5$ and $(a_3), (b_3)$ $t=25$ (density spread maxima) after the quench shown in Fig. 3.6.

particles, $c_0 = 1$ and initial AF state, $|g_1^{(1)}(x, x'; t)|$ is shown in Fig. 3.9(a_1) – 3.9(a_3). Interestingly, for our system the one-body coherence remains the same for different values of σ , thus being independent of the particle's spin state. Moreover, the features emerging in the one-body coherence remain robust during the evolution, except for the expansion of the density cloud as one goes from the density spread minima to maxima (compare Fig. 3.9(a_1) – 3.9(a_3)). Comparing the positions of these filaments and the one-body coherence we find that the particle for coordinates within the filament region are coherent, see the bright blocks at the diagonal near the centre of the trap eg. $g_1^{(1)}(x = -2, x' = -2; t = 1) \approx 1$ in Fig. 3.9(a_1). While we find that for coordinates corresponding to neighbouring filaments we have a substantial loss of coherence, see the off diagonal region near the centre of trap eg. $g_1^{(1)}(x = -2, x' = 3; t = 1) \approx 0.88$ in Fig. 3.9(a_1).

Having explored the one-body correlations, we now discuss the normalized two-body correla-

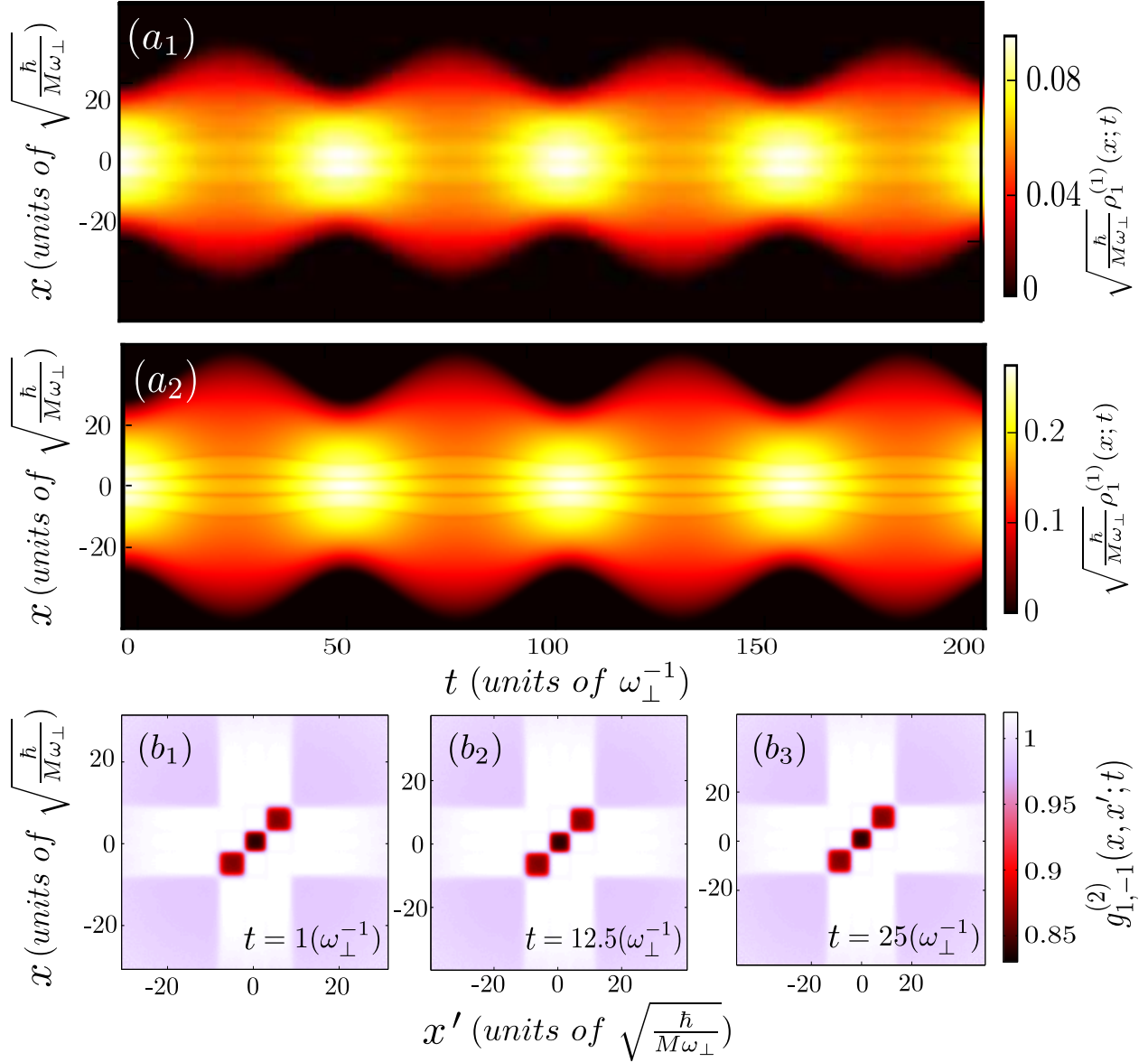


Figure 3.10: (a₁) and (a₂) are the beyond mean field spatiotemporal evolution of the $f_z = 1$ one body density $\rho_1^{(1)}(x;t)$ for the AF state of $N = 50$ particles with $c_0 = 1$ and $c_0 = 5$ respectively, after the quench. Here $p/c_1 n = 0.04$, $q/c_1 n = -0.44$ and $c_1 = 0.018$. (b₁), (b₂), (b₃) refer to the two body correlations $g_{1,-1}^{(2)}(x_1, x_2; t)$ for, (b₁) $t=1$ (density spread minima), (b₂) $t=12.5$ and (b₃) $t=25$ (density spread maxima) after the quench.

tion function

$$g_{\sigma\sigma'}^{(2)}(x, x'; t) = \frac{\rho_{\sigma\sigma'}^{(2)}(x, x'; t)}{\sqrt{\rho_\sigma^{(1)}(x; t) \rho_{\sigma'}^{(1)}(x'; t)}}. \quad (3.3)$$

Here $\rho_{\sigma\sigma'}^{(2)}(x, x'; t_o) = \langle \Psi(t_o) | \hat{\Psi}_\sigma^\dagger(x) \hat{\Psi}_{\sigma'}^\dagger(x') \hat{\Psi}_{\sigma'}(x') \hat{\Psi}_\sigma(x) | \Psi(t_o) \rangle$ is the diagonal two-body reduced density matrix. We note that a perfectly condensed MB state leads to $|g_{\sigma\sigma'}^{(2)}(x, x'; t)| = 1$ which is termed as an uncorrelated state. While, $|g_{\sigma\sigma'}^{(2)}(x, x'; t)|$ smaller(larger) than unity is termed as an anti-correlated(correlated) state. For our system $\sigma \neq \sigma'$ corresponds to correlations between particles in different spin states while $\sigma = \sigma'$ refers to the two body correlations for particles in the same spin state. In Fig. 3.9(b_1) – 3.9(b_3) we show the two body correlation function, $g_{\sigma\sigma'}^{(2)}(x, x'; t)$ for the quench of the AF state presented in Fig. 3.6. Interestingly, for our system the correlation function turns out to be independent of the σ and σ' and preserves its structure during the evolution, while expanding and contracting (not shown here for brevity) in size, similar to one-body correlation function following the density spreading and contraction. Comparing the positions, we find that two particles within the filament are anti correlated, see the dark blocks at the diagonal near the centre of trap eg. $g_{1,-1}^{(2)}(x = -2, x' = -2; t = 1) \approx 0.9$ in Fig. 3.9(b_1). While, the particles belonging to neighbouring filaments are correlated to each other, see the bright white patches near the off diagonal region eg. $g_{1,-1}^{(2)}(x = -2, x' = 3; t = 1) \approx 1.03$ in Fig. 3.9(b_1).

Turning our attention to stronger interactions, we observe that upon increasing c_0 to 5 the filaments become more prominent, see Fig. 3.10(a_2). Furthermore, the number of filaments is also increased from 2 for $c_0 = 1$ Fig. 3.10(a_1) to 3 for $c_0 = 5$ Fig. 3.10(a_2). Note here that for brevity, we only show the particle density corresponding to the $f_z = 1$ state, though the $f_z = -1$ state is also occupied since we have quenched an initially AF state, similar to Fig. 3.6. Furthermore for $c_0 = 5$, the two-body correlations exhibit three block like anti correlated structures each of which corresponds to a filament, see the dark block structures along the diagonal eg. $g_{1,-1}^{(2)}(x = 5, x' = 5; t = 1) \approx 0.85$ in Fig. 3.10(b_1). This in contrast to the two block structure observed for $c_0 = 1$, see Fig. 3.9(b_1) – 3.9(b_3). Additionally the neighbouring eg. $g_{1,-1}^{(2)}(x = -5, x' = 0.7; t = 1) = 1.025$, as well as, the next neighbouring filaments eg. $g_{1,-1}^{(2)}(x = -5, x' = 5; t = 1) = 1.02$ are slightly correlated to each other, see the off diagonal bright white region in Fig. 3.9(b_1) – 3.9(b_3). Another interesting observation is the increased number of filaments, 4 in $N=20$ particles [Fig. 3.11(a_2)] compared to 2 for $N=50$ particles [Fig. 3.11(a_1)]. This behavior is also imprinted in the two body correlation function [Fig. 3.11(b_1) – 3.11(b_3)] where we observe presence of four prominent anti correlated blocks pattern each of which correspond to a filament. This is in contrast to the two anti correlated block structure for $N = 50$ particles Fig. 3.9(b_1) – 3.9(b_3). Also, we can identify presence of correlations between the neighbouring filaments, see the bright off diagonal region eg. $g_{1,-1}^{(2)}(x = -1.7, x' = 2.5; t = 1 \approx 1.08)$ in Fig. 3.11(b_1) – 3.11(b_3). Moreover, we find that the correlation decreases for next neighbouring and next to next neighbouring filaments, as the intensity of the bright region decreases as one moves away from the diagonal in Fig. 3.11(b_1) –

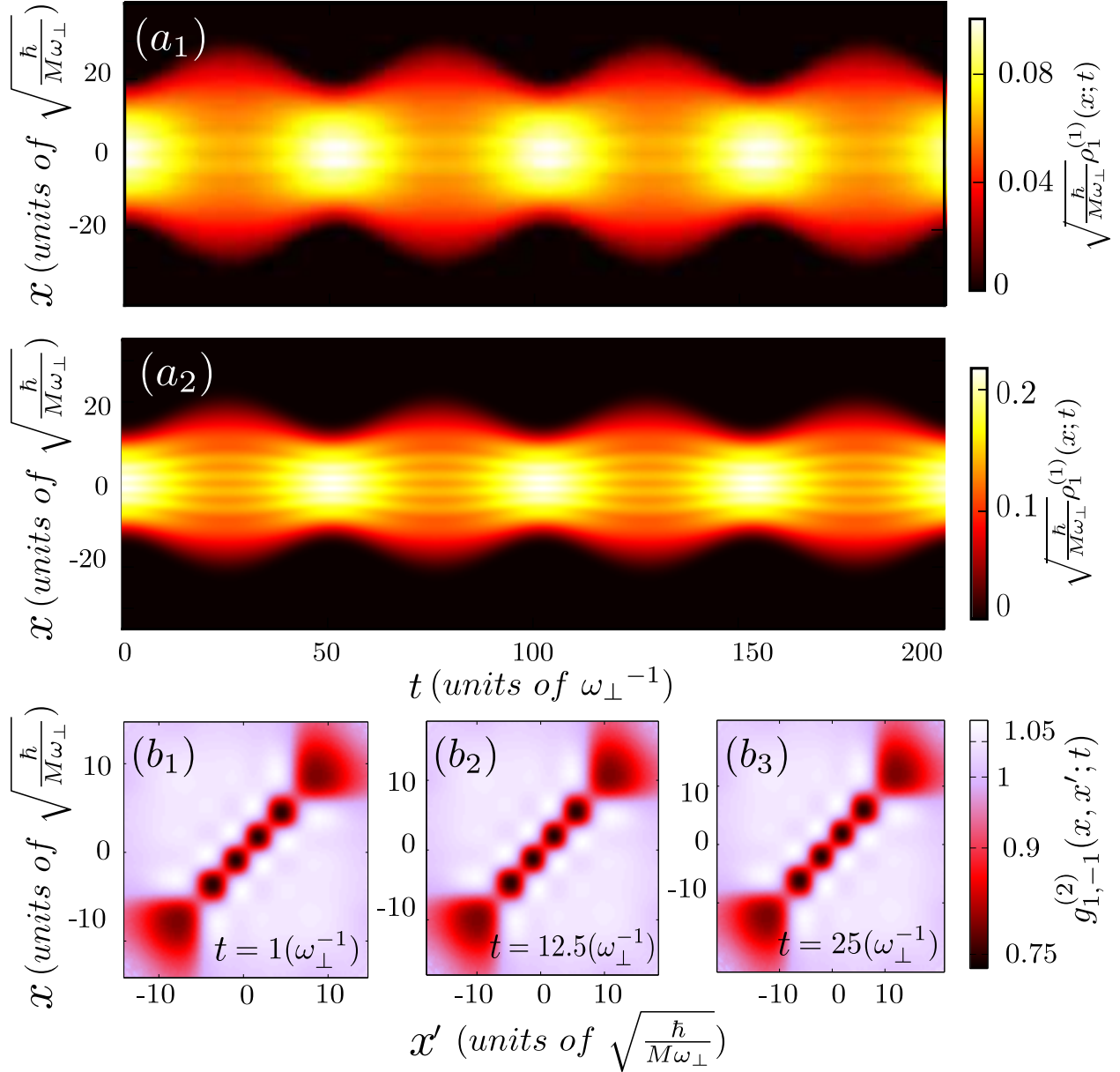


Figure 3.11: (a₁) and (a₂) are the beyond mean field spatiotemporal evolution of the f_z one body densities $\rho_1^{(1)}(x;t)$ for the AF state of $N = 50$ and $N = 20$ particles respectively, after an abrupt quench of the trapping frequency from $\omega = 0.1$ to $\omega = 0.07$, here $p/c_1n = 0.04$, $q/c_1n = -0.44$, $g_o = 1$ and $c_1 = 0.018$. (b₁), (b₂), (b₃) are the two body correlations $g_{1,-1}^{(2)}(x, x'; t)$ for, (b₁) $t=1$ (density spread minima), (b₂) $t=12.5$ and (b₃) $t=25$ (density spread maxima) after the quench.

3.11(b₃) eg. compare $g_{1,-1}^{(2)}(x = -1.7, x' = 2.5; t = 1) \approx 1.08$ to $g_{1,-1}^{(2)}(x = -3.7, x' = 2.5; t = 1) \approx 1.04$. Additionally, we have measured that the period of the breathing mode remains the same for both $N = 50$ and $N = 20$ particles.

Chapter 4

Conclusions and Outlook

In the present work we have explored the ground state properties as well as the dynamics induced by an abrupt shift of the confinement frequency for a spin-1 Bose gas. Regarding the ground state properties, we have studied how the phase diagram of these systems is altered when one takes correlations into account and thus operates beyond the mean-field approximation. Furthermore, the effect of the finite size of the system on the boundaries between the different phases was investigated. For examining the quench dynamics, we have relied on the dynamical behaviour of the one and two-body distributions for the different involved spin states and characterized the correlation induced effects by comparing the response within and beyond the mean field approximation. Additionally, significant changes of this behavior were revealed for different total particle numbers, as well as, interaction strengths.

In our study of the different phases emanating in our system we have found that even though the incorporation of correlations does not lead to a substantial change in the boundaries referring to first order transitions, the second order ones are significantly altered. We observe that for both ferromagnetic and anti-ferromagnetic spin-spin interactions, the transition boundaries get shifted leading to a decreased window in terms of p , and q where the AF and BA phases are accessed. Note here that both of the above mentioned phases are characterized by a superposition state in terms of the involved spin-states demonstrating that correlated systems favor ground states where the bosons get polarized in a single f_z state. Additionally, by comparing the phase boundaries corresponding to second order transitions for $N = 5, 20$ and 50 particles, we have found that the correlation effects on the phase diagram become more prominent as one decreases the number of

particles. By simulating $N = 500$ particles in the mean field approximation we have recovered the thermodynamic limit associated with the decoupling of the spin and spatial states, a result which reveals the importance of the interplay of these degrees of freedom for setups with finite particle numbers.

The quench of the trapping frequency induced a breathing motion into the system with the frequency of this oscillation being independent of the spin state and the phase of the system. Interestingly, for an initial BA state we have even observed spin flip dynamics which involves $f_z = \pm 1$ particles that coherently get transferred to the $f_z = 0$ state and vice versa. Moreover, we have found that the incorporation of correlations leads to the formation of filament-like high density regions. The number of these filaments increased from 2 to 3 when we changed the spin-independent interaction parameter from $c_0 = 1$ to $c_0 = 5$. Similarly, an increase of the number of filaments was also observed when the particle number was decreased from $N = 50$ to $N = 20$.

To further quantify the effect of correlations, we have inspected the time evolution of the one-body and the two-body correlation functions. We revealed that coherence is maintained within each filament during the dynamics, while significant losses of coherence occur between the neighbouring filaments. Moreover, irrespective of the interaction strength and particle number, two particles within a filament exhibit an anti-correlated character while, particles between neighbouring filaments are correlated to each other throughout the dynamical evolution.

Having explored the rich physics associated with spin-1 Bose gas because of the finite size effects and incorporation of correlations. One can further explore the corresponding alterations in phase space and the dynamical properties for spin-2 and spin-3 Bose gas systems. It can also be interesting to study a quench of the interaction parameter so that we can study the dynamical effects following a sudden change in the phase space region of the system. Other quench studies can include a sudden change in the direction of magnetic field, as well as, a combination of above proposed quenches.

Chapter 5

Appendix

5.1 Natural Population

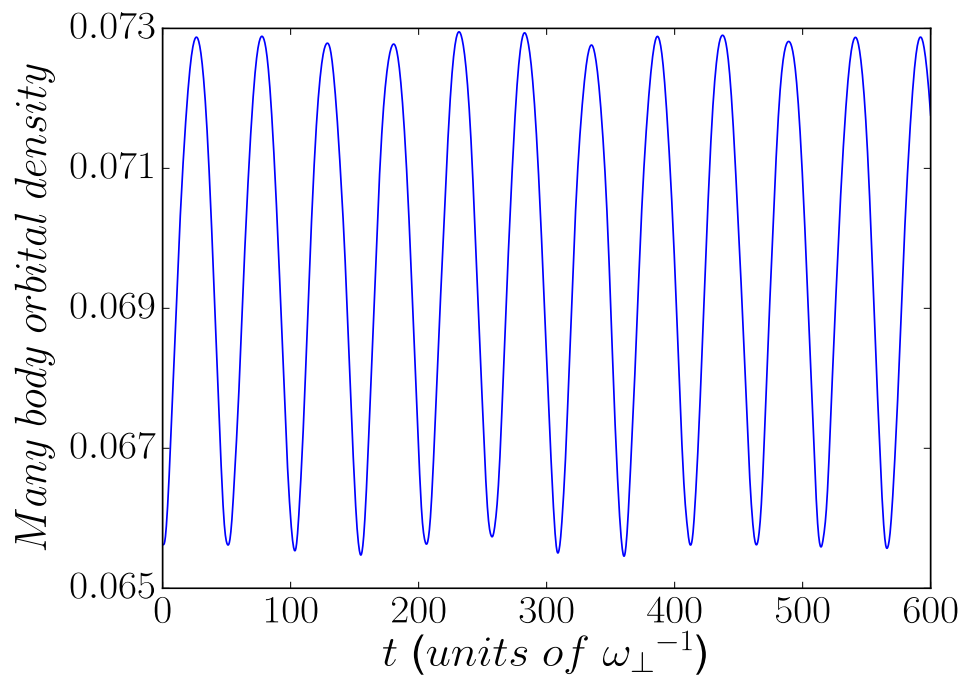


Figure 5.1: Population density of beyond mean field orbitals for $N = 50$ particles for the phase quench discussed in Fig.3.6.

In this section we show the beyond mean orbital orbital occupation for our phase space and quench analysis. The substantial occupation of these orbitals indicate the presence of important

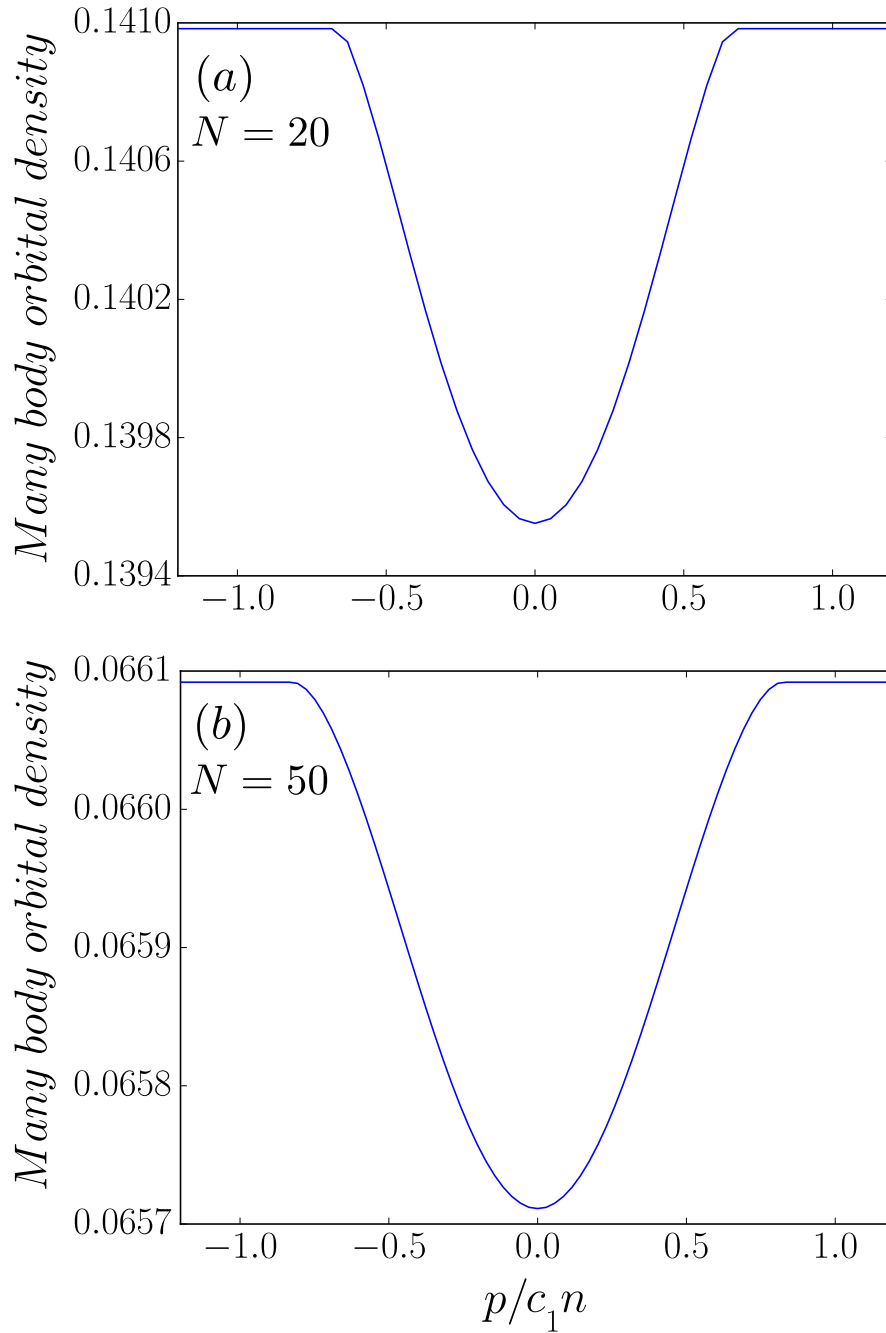


Figure 5.2: Population density of beyond mean field orbitals for (a) $N = 20$ and (b) $N = 50$ particles for the phase space region discussed in Fig.3.3(a). The behavior shown is for fixed $q/c_1 n = 0.5$ and varying $p/c_1 n$.

unexplored physics which is not detected in the earlier did mean field analysis. In Fig.5.2 we show the beyond mean field orbital occupation for the phase space region discussed in Fig.3.3(a). We see that there is substantially occupation of orbitals corresponding to beyond mean field limit.

Moreover, comparing the respective y-axis, one can infer that the orbital density is considerably more for $N = 20$ particles compared to $N = 50$ particles. This behavior is in direct relation to the results discussed above. As we see the phase space changes due to incorporation of correlations are greater as the particle number decreases.

In Fig.5.1 we show the beyond mean field orbital occupation for the dynamic behavior for a quench in the trapping frequency discussed in Fig.3.6. We find that the orbital density show a interesting behaviour as there population density oscillates similar to the breathing mode oscillation induced in the system because of the quench. Further, comparing $N = 20$ and $N = 50$ particles, we see that the presence of prominent and more number of filaments in $N = 20$ case is also evident in the higher beyond mean field orbital occupation for the same.

We saw the convergence of beyond mean field orbitals as the computation accuracy was increased. Considering this, we choose the appropriate accuracy for our simulations so that we could correctly capture the beyond mean field effects for our system.

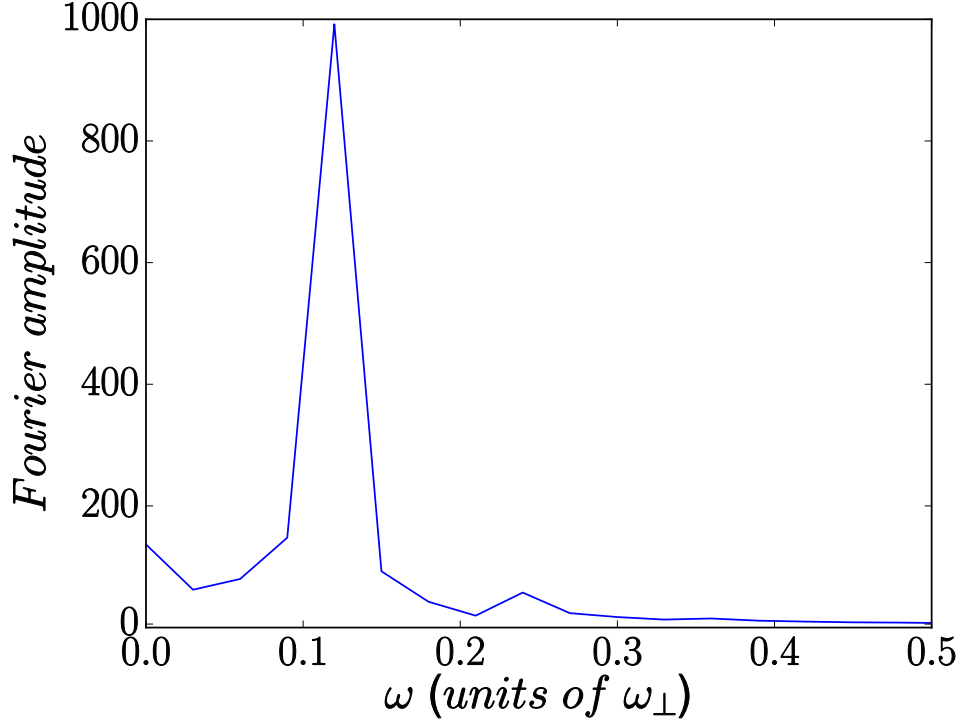


Figure 5.3: Amplitude for the Fourier transform of the breathing oscillation shown particles in $f_z = 1$ state for the quench shown in Fig. 3.6.

5.2 Quench analysis

Here we show the amplitude for the Fourier transform of the breathing mode oscillation. Further, we also show the density evolution for particles initially in $f_z = 1$ state after a quench in the trapping frequency for an initially F2 state.

In Fig. 5.4 we show the Fourier amplitude for the frequency of the breathing oscillation shown in Fig. 3.6 for the particles in the spin state $f_z = 1$. We see that the Fourier amplitude is strongly peaked at $\omega = 0.12$ which was also reported in Section 3.2. Further, we had similar peak for particles in all the initial states which include F1,F2,AF,P and BA phase, as well as, different spin states. A strong peak at $\omega = 0.12$ was also shown by $N = 20$ particles, as well as, $N = 5$ particles. Moreover, a change in the interaction from $c_0 = 1$ to $c_0 = 5$ also did not lead to a change in the frequency of the breathing oscillation. Thus the system shows interesting behavior with the frequency of breathing oscillation being independent of initial phase space state, spin state, the particle number, as well as, the system's interactions. Further, we saw that the frequency of the breathing oscillation did change when we tuned the amount of the change in the trapping frequency.

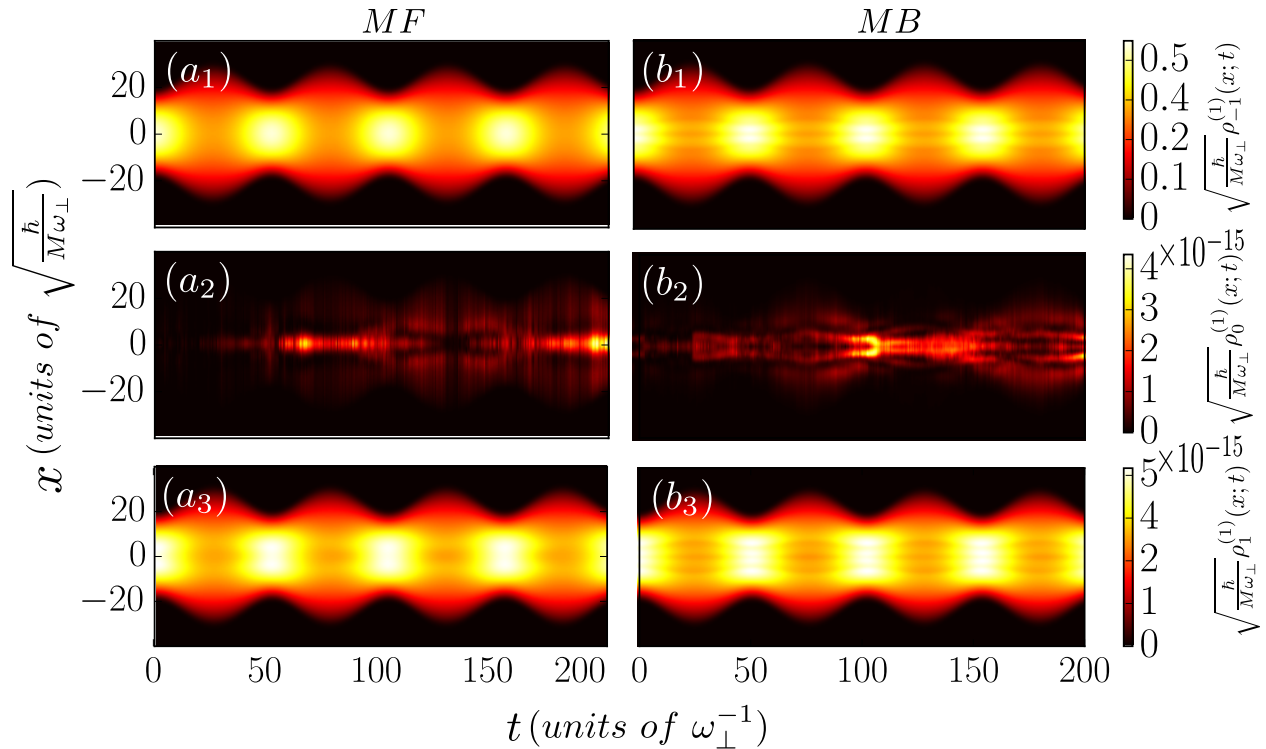


Figure 5.4: Amplitude for the Fourier transform of the breathing oscillation shown particles in $f_z = 1$ state for the quench shown in Fig. 3.6.

In Fig. 5.3 we show the quench induced dynamics for F2 state. As expected, we have significant occupation of only $f_z = -1$ state throughout the dynamics (note the color-bar scale for $f_z = 0$ and $f_z = 1$ spin state is insignificant). We see that here we do not see any spin flip dynamics, such dynamics was only seen when initially all the three spin states were occupied such as in BA state. Further, we also note that the oscillation to be same as for the AF (Fig. 3.6) and BA (Fig. 3.7) state i.e $\omega = 0.12$ for the breathing motion. Similar corresponding behavior was also seen for a quench of an initially F1 and P state.

Bibliography

- [1] D. M. Stamper-Kurn, M. R. Andrews, A. P. Chikkatur, S. Inouye, H.-J. Miesner, J. Stenger, and W. Ketterle, “Optical confinement of a bose-einstein condensate,” *Phys. Rev. Lett.*, vol. 80, pp. 2027–2030, Mar 1998.
- [2] T.-L. Ho, “Spinor bose condensates in optical traps,” *Phys. Rev. Lett.*, vol. 81, pp. 742–745, Jul 1998.
- [3] A. T. Black, E. Gomez, L. D. Turner, S. Jung, and P. D. Lett, “Spinor dynamics in an antiferromagnetic spin-1 condensate,” *Phys. Rev. Lett.*, vol. 99, p. 070403, Aug 2007.
- [4] Y. Kawaguchi and M. Ueda, “Spinor bose–einstein condensates,” *Physics Reports*, vol. 520, p. 253–381, Nov 2012.
- [5] D. M. Stamper-Kurn and M. Ueda, “Spinor bose gases: Explorations of symmetries, magnetism and quantum dynamics,” *arXiv*, 1205.1888, 2012.
- [6] J. Stenger, S. Inouye, D. M. Stamper-Kurn, H.-J. Miesner, A. P. Chikkatur, and W. Ketterle, “Spin domains in ground-state bose–einstein condensates,” *Nature*, vol. **396**, no. 6709, p. 345, (1998).
- [7] C. V. Ciobanu, S.-K. Yip, and T.-L. Ho *Phys. Rev. A*, vol. 61, p. 033607, Feb 2000.
- [8] M. Ueda and M. Koashi, “Theory of spin-2 bose-einstein condensates: Spin correlations, magnetic response, and excitation spectra,” *Phys. Rev. A*, vol. 65, p. 063602, May 2002.
- [9] R. B. Diener and T.-L. Ho, “ ^{52}Cr spinor condensate: A biaxial or uniaxial spin nematic,” *Phys. Rev. Lett.*, vol. 96, p. 190405, May 2006.
- [10] M.-S. Chang, C. D. Hamley, M. D. Barrett, J. A. Sauer, K. M. Fortier, W. Zhang, L. You, and M. S. Chapman, “Observation of spinor dynamics in optically trapped ^{87}Rb bose-einstein condensates,” *Phys. Rev. Lett.*, vol. 92, p. 140403, Apr 2004.
- [11] H. Schmaljohann, M. Erhard, J. Kronjäger, M. Kottke, S. van Staa, L. Cacciapuoti, J. J. Arlt, K. Bongs, and K. Sengstock, “Dynamics of $f = 2$ spinor bose-einstein condensates,” *Phys. Rev. Lett.*, vol. 92, p. 040402, Jan 2004.

- [12] T. Kuwamoto, K. Araki, T. Eno, and T. Hirano, “Magnetic field dependence of the dynamics of ^{87}Rb spin-2 bose-einstein condensates,” *Phys. Rev. A*, vol. 69, p. 063604, Jun 2004.
- [13] B. Pasquiou, E. Maréchal, G. Bismut, P. Pedri, L. Vernac, O. Gorceix, and B. Laburthe-Tolra, “Spontaneous demagnetization of a dipolar spinor bose gas in an ultralow magnetic field,” *Phys. Rev. Lett.*, vol. 106, p. 255303, Jun 2011.
- [14] J. Jie, Q. Guan, and D. Blume, “Spinor bose-einstein condensate interferometer within the undepleted pump approximation: Role of the initial state,” *Phys. Rev. A*, vol. 100, p. 043606, Oct 2019.
- [15] P. Tang, X. Dong, W. Zhang, Y. Li, X. Chen, and X. Zhou, “Implementation of a double-path multimode interferometer using a spinor bose-einstein condensate,” *Phys. Rev. A*, vol. 101, p. 013612, Jan 2020.
- [16] Z. Li, C. Bao, and W. Zheng, “Hyperfine state entanglement of spinor BEC and scattering atom,” *Journal of Physics B: Atomic, Molecular and Optical Physics*, vol. 51, p. 095301, apr 2018.
- [17] P. Xu, S. Yi, and W. Zhang, “Efficient generation of many-body entangled states by multilevel oscillations,” *Phys. Rev. Lett.*, vol. 123, p. 073001, Aug 2019.
- [18] A. E. Leanhardt, Y. Shin, D. Kielpinski, D. E. Pritchard, and W. Ketterle, “Coreless vortex formation in a spinor bose-einstein condensate,” *Phys. Rev. Lett.*, vol. 90, p. 140403, Apr 2003.
- [19] P. G. Kevrekidis, H. Susanto, R. Carretero-González, B. A. Malomed, and D. J. Frantzeskakis, “Vector solitons with an embedded domain wall,” *Phys. Rev. E*, vol. 72, p. 066604, Dec 2005.
- [20] H. E. Nistazakis, D. J. Frantzeskakis, P. G. Kevrekidis, B. A. Malomed, R. Carretero-González, and A. R. Bishop, “Polarized states and domain walls in spinor bose-einstein condensates,” *Phys. Rev. A*, vol. 76, p. 063603, Dec 2007.
- [21] P. G. Kevrekidis, H. Susanto, R. Carretero-González, B. A. Malomed, and D. J. Frantzeskakis, “Vector solitons with an embedded domain wall,” *Phys. Rev. E*, vol. 72, p. 066604, Dec 2005.
- [22] H. E. Nistazakis, D. J. Frantzeskakis, P. G. Kevrekidis, B. A. Malomed, R. Carretero-González, and A. R. Bishop, “Polarized states and domain walls in spinor bose-einstein condensates,” *Phys. Rev. A*, vol. 76, p. 063603, Dec 2007.
- [23] S. Gautam and S. K. Adhikari, “Three-dimensional vortex-bright solitons in a spin-orbit-coupled spin-1 condensate,” *Phys. Rev. A*, vol. 97, p. 013629, Jan 2018.
- [24] S. Li, B. Prinari, and G. Biondini, “Solitons and rogue waves in spinor bose-einstein condensates,” *Phys. Rev. E*, vol. 97, p. 022221, Feb 2018.

- [25] T. M. Bersano, V. Gokhroo, M. A. Khamehchi, J. D’Ambroise, D. J. Frantzeskakis, P. Engels, and P. G. Kevrekidis, “Three-component soliton states in spinor $f = 1$ bose-einstein condensates,” *Phys. Rev. Lett.*, vol. 120, p. 063202, Feb 2018.
- [26] “Observation of universal dynamics in a spinor bose gas far from equilibrium.,”
- [27] P. Kunkel, M. Prüfer, S. Lannig, R. Rosa-Medina, A. Bonnin, M. Gärttner, H. Strobel, and M. K. Oberthaler, “Simultaneous readout of noncommuting collective spin observables beyond the standard quantum limit,” *Phys. Rev. Lett.*, vol. 123, p. 063603, Aug 2019.
- [28] M. Prüfer, T. V. Zache, P. Kunkel, S. Lannig, A. Bonnin, H. Strobel, J. Berges, and M. K. Oberthaler, “Experimental extraction of the quantum effective action for a non-equilibrium many-body system,” 2019.
- [29] W. Zhang, S. Yi, and L. You, “Mean field ground state of a spin-1 condensate in a magnetic field,” *New Journal of Physics*, vol. 5, pp. 77–77, jun 2003.
- [30] K. Murata, H. Saito, and M. Ueda, “Broken-axisymmetry phase of a spin-1 ferromagnetic bose-einstein condensate,” *Phys. Rev. A*, vol. 75, p. 013607, Jan 2007.
- [31] D. Jacob, L. Shao, V. Corre, T. Zibold, L. De Sarlo, E. Mimoun, J. Dalibard, and F. Gerbier, “Phase diagram of spin-1 antiferromagnetic bose-einstein condensates,” *Phys. Rev. A*, vol. 86, p. 061601, Dec 2012.
- [32] D. M. Stamper-Kurn, H.-J. Miesner, A. P. Chikkatur, S. Inouye, J. Stenger, and W. Ketterle, “Quantum tunneling across spin domains in a bose-einstein condensate,” *Phys. Rev. Lett.*, vol. 83, pp. 661–665, Jul 1999.
- [33] H. Saito and M. Ueda, “Diagnostics for the ground-state phase of a spin-2 bose-einstein condensate,” *Phys. Rev. A*, vol. 72, p. 053628, Nov 2005.
- [34] L. He and S. Yi, “Magnetic properties of a spin-3 chromium condensate,” *Phys. Rev. A*, vol. 80, p. 033618, Sep 2009.
- [35] “Spontaneous symmetry breaking in a quenched ferromagnetic spinor bose–einstein condensate,”
- [36] S. R. Leslie, J. Guzman, M. Vengalattore, J. D. Sau, M. L. Cohen, and D. M. Stamper-Kurn, “Amplification of fluctuations in a spinor bose-einstein condensate,” *Phys. Rev. A*, vol. 79, p. 043631, Apr 2009.
- [37] E. M. Bookjans, A. Vinit, and C. Raman, “Quantum phase transition in an antiferromagnetic spinor bose-einstein condensate,” *Phys. Rev. Lett.*, vol. 107, p. 195306, Nov 2011.
- [38] S. De, D. L. Campbell, R. M. Price, A. Putra, B. M. Anderson, and I. B. Spielman, “Quenched binary bose-einstein condensates: Spin-domain formation and coarsening,” *Phys. Rev. A*, vol. 89, p. 033631, Mar 2014.

- [39] S. Kang, D. Hong, J. H. Kim, and Y. Shin, “Crossover from weak to strong quench in a spinor bose-einstein condensate,” *Physical Review A*, vol. 101, Feb 2020.
- [40] R. Schmitz, S. Krönke, L. Cao, and P. Schmelcher, “Quantum breathing dynamics of ultracold bosons in one-dimensional harmonic traps: Unraveling the pathway from few- to many-body systems,” *Phys. Rev. A*, vol. 88, p. 043601, Oct 2013.
- [41] M. Pyzh, S. Krönke, C. Weitenberg, and P. Schmelcher, “Spectral properties and breathing dynamics of a few-body bose–bose mixture in a 1d harmonic trap,” *New Journal of Physics*, vol. 20, p. 015006, jan 2018.
- [42] S. I. Mistakidis, G. C. Katsimiga, P. G. Kevrekidis, and P. Schmelcher, “Correlation effects in the quench-induced phase separation dynamics of a two species ultracold quantum gas,” *New Journal of Physics*, vol. 20, p. 043052, apr 2018.
- [43] G. I. Mias, N. R. Cooper, and S. M. Girvin, “Quantum noise, scaling, and domain formation in a spinor bose-einstein condensate,” *Phys. Rev. A*, vol. 77, p. 023616, Feb 2008.
- [44] S. I. Mistakidis, G. C. Katsimiga, G. M. Koutentakis, T. Busch, and P. Schmelcher, “Quench dynamics and orthogonality catastrophe of bose polarons,” *Phys. Rev. Lett.*, vol. 122, p. 183001, May 2019.
- [45] A. Romero-Ros, G. C. Katsimiga, P. G. Kevrekidis, and P. Schmelcher, “Controlled generation of dark-bright soliton complexes in two-component and spinor bose-einstein condensates,” *Phys. Rev. A*, vol. 100, p. 013626, Jul 2019.
- [46] D. J. Papoular, G. V. Shlyapnikov, and J. Dalibard, “Microwave-induced fano-feshbach resonances,” *Phys. Rev. A*, vol. 81, p. 041603, Apr 2010.
- [47] L. Cao, V. Bolsinger, S. I. Mistakidis, G. M. Koutentakis, S. Krönke, J. M. Schurer, and P. Schmelcher, “A unified ab initio approach to the correlated quantum dynamics of ultracold fermionic and bosonic mixtures,” *The Journal of Chemical Physics*, vol. 147, no. 4, p. 044106, 2017.
- [48] V. J. Bolsinger, S. Krönke, and P. Schmelcher, “Beyond mean-field dynamics of ultra-cold bosonic atoms in higher dimensions: facing the challenges with a multi-configurational approach,” *Journal of Physics B: Atomic, Molecular and Optical Physics*, vol. 50, p. 034003, jan 2017.